

UC San Diego

UC San Diego Electronic Theses and Dissertations

Title

Towards Brain Decoding for Real-World Drowsiness Detection

Permalink

<https://escholarship.org/uc/item/6zq154xw>

Author

Wei, Chun-Shu

Publication Date

2017

Peer reviewed|Thesis/dissertation

UNIVERSITY OF CALIFORNIA, SAN DIEGO

Towards Brain Decoding for Real-World Drowsiness Detection

A dissertation submitted in partial satisfaction of the
requirements for the degree Doctor of Philosophy

in

Bioengineering

by

Chun-Shu Wei

Committee in charge:

Professor Tzyy-Ping Jung, Chair
Professor Gert Cauwenberghs, Co-Chair
Professor Chung-Kuan Cheng
Professor Virginia de Sa
Professor Gabriel Silva

2017

Copyright

Chun-Shu Wei, 2017

All rights reserved.

The Dissertation of Chun-Shu Wei is approved, and is acceptable in quality and form for publication on microfilm and electronically:

Co-Chair

Chair

University of California, San Diego

2017

EPIGRAPH

*In darkness, cold.
In light, cold.
The old sun brings no heat.
But there is heat in breath and life.
In life, there is the Force.
In the Force, there is life.
And the Force is eternal.*

—Sunset Prayer of the Guardians of the Whills

TABLE OF CONTENTS

Signature Page	iii
Epigraph	iv
Table of Contents	v
List of Figures	viii
List of Tables	xi
Acknowledgements	xii
Vita	xiv
Abstract of the Dissertation	xvii
Chapter 1 Introduction	1
Chapter 2 Associations between EEG Dynamics and Drowsiness and their Variability across Subjects and Sessions	9
2.1 Background.....	9
2.2 Materials and Methods	11
2.2.1 Behavioral Analysis.....	12
2.2.2 EEG Recording and Processing.....	14
2.2.3 EEG Feature Extraction.....	15
2.2.4 Hierarchical Cluster Analysis.....	16
2.3 Results.....	17
2.4 Discussion.....	20
2.5 Conclusion.....	21
Acknowledgements.....	22
Chapter 3 Drowsiness Detection Using Non-Hair-Bearing EEG-Based Brain-Computer Interfaces.....	23
3.1 Background.....	24
3.2 Materials and Methods	27
3.2.1 Behavioral Data Labeling.....	27
3.2.2 EEG Processing	27
3.2.3 EEG Feature Extraction.....	28

3.2.4	EEG Classification.....	29
3.4	Results.....	31
3.5	Conclusion.....	41
	Acknowledgments.....	41
Chapter 4	A Subject-Transfer Framework for Plug-and-Play Drowsiness Detection.....	42
4.1	Background.....	43
4.2.1	EEG-DI Regression Models.....	49
4.2.2	Multiple Distance Measurements.....	50
4.2.3	Source Model Ranking.....	53
4.2.4	Model Fusion and Re-Calibration.....	54
4.3	Results.....	55
4.4	Discussion.....	61
4.5	Conclusion.....	64
	Acknowledgments.....	64
Chapter 5	Conclusion and Future Works.....	66
Appendix A	Selective Transfer Learning for EEG-Based Drowsiness Detection.....	68
A.1	Background.....	69
A.2	Materials and Methods.....	70
A.2.1	Experiment and Participants.....	70
A.2.2	EEG Dataset and Preprocessing.....	71
A.2.3	Estimation of Drowsiness Level.....	71
A.2.4	EEG Feature Extraction.....	72
A.2.5	EEG-Based Drowsiness Regression Model.....	72
A.2.6	Level of Session Generalizability.....	73
A.2.7	Selecting Auxiliary Sessions for Transfer Learning.....	74
A.2.8	Selective transfer Learning and Performance Evaluation.....	75
A.3	Results.....	75
A.4	Discussions and Conclusion.....	78
A.5	Acknowledgement.....	79

Appendix B Exploring the EEG Correlates of Drowsiness with Robust Principal Component Analysis	81
B.1 Background.....	81
B.2 Materials and Methods	83
B.2.1 Experiment and EEG Recording	83
B.2.2 Experiment and EEG Recording	84
B.2.3 EEG Data Processing	84
B.2.4 Robust Principal Component Analysis.....	85
B.3 Results and Discussion	86
B.4 Conclusion.....	91
B.5 Acknowledgement.....	92
Bibliography	93

LIST OF FIGURES

Figure. 2.1: (a) The experimental paradigm of the lane-keeping driving task; (b) Change of the RT and the RT-based DI across a sample session (S41-4) 14

Figure. 2.2: (a) Topography of spatial distributions of EEG band powers in the alert and drowsy states; (b) EEG-DI correlation of a sample session (S41-4); (c) Scatter plots of EEG band powers against DI at representative channels along the midline, Fz, Cz, Pz, and Oz. 17

Figure. 2.3: The topography of EEG-DI correlations in sessions S5-1 and S5-2. Drastic discrepancy appears in the EEG-DI correlations in the alpha band (a strong positive correlation across the whole scalp in session 1 versus a strong negative correlation in session 2 from the same subject). 18

Figure. 2.4: Hierarchically clustered sessions (rows) and EEG power features (columns) with dendrograms across 54 sessions from 25 subjects who experienced drowsiness in the LKT experiments. 19

Figure. 3.1: (a) The partition of hair-covered areas and non-hair-bearing area divided by a brown boundary. (b) The layout of electrode locations of the 32-channel recording system. Brown boundary separates the divisions of hair-covered and non-hair-bearing area. 28

Figure. 3.2: The scalp topography of correlation distributions that exhibits the correlation coefficients (ρ) between normalized RT and pre-event EEG power features of theta, alpha, and beta band at different channel locations across subjects. 31

Figure. 3.3: EEG spectral changes from alertness to drowsiness at different representative channels and frequency bands. 32

Figure. 3.4: (a) The change of global RT across an entire session of subject 9. (b) The classification results of drowsiness detection using three types of classifier (SVM, LDA, and k NN) with NHB and AC EEG for the same session as in (a). 35

Figure. 3.5: ROC curves describing the relation between true positive rate (sensitivity) and false positive rate (specificity) using NHB EEG and AC EEG with different classifiers on subject 9. Note that positive refers to drowsiness....	36
Figure 4.1: An illustration of the proposed subject-transfer framework. A source model pool is constructed based on the existing data collected from the source (other) subjects.	50
Figure 4.2: The training and test flow of the transferability model for source model ranking.	54
Figure 4.3: Actual (blue bars) and predicted (red bars) transferability scores of source models based on the alert baseline similarity among subjects.	57
Figure 4.4: EEG-based DI decoding result using self-decoding (SD) and subject-transfer (ST) approaches with LR and SVR of a sample session (S54-2).	58
Figure 4.5: The decoding performance of the proposed subject-transfer (ST) approach (the red curve with standard error) as a function of the number of source subjects available in the pool. The gray curve shows the randomized ST performance without source-model ranking.	59
Figure 4.6: A comparison of decoding performance between using the proposed subject-transfer (ST) and the conventional self-decoding (SD) approach in terms of decoding performance (correlation coefficient, ρ), and calibration time across 17 target subjects who performed multiple LKT sessions.	60
Figure A.1: The performance improvement with transfer learning as a function of the level of session generalizability (LSG). The significantly negative correlation implies that a pilot model with lower LSG value benefited more from applying transfer learning approach to estimate the drowsiness level.	77
Figure A.2: The performances of TL-augmented sessions (with $LSG < 1$) as a function of the number of auxiliary sessions involved. The performance based on within-subject validation was also provided for comparison.	77
Figure A.3: The performance using the proposed selective TL, TL (non-selective), and within-subject cross-session validation.	78

Figure B.1: Time series of RTs before and after RT normalization in two representative subjects. (a) the conversion from RT to the proposed lapse index with alert RT = 0.6 s. (b) the time series of original RTs in Subjects S1 and S2, and (c) the time series of the lapse index after RT normalization. 89

Figure B.2: The statistical significance of the correlations (log *p*-value) between RTs and band power using (from the top) the band-passed EEG signals (original), sparse components, and low-rank components at different scalp locations. 90

Figure B.3: The average correlation coefficients between band power and RTs at four representative scalp locations (Fz, Cz, Pz, and Oz) using the band-passed EEG signals (Original), sparse components (S), and low-rank components (L). 91

LIST OF TABLES

Table 3.1 Power Difference of EEG Features between Alert and Drowsy State.....	34
Table 3.2 Overall Accuracy of Drowsiness Detection using Within-Subject Cross- Session Validation	34
Table 4.1 Representative studies dedicated to calibration time reduction for brain decoding.....	44
Table 4.2 Overall decoding performance using different approaches.....	58

ACKNOWLEDGEMENTS

This would not happen without the guidance of my committee member, help from colleagues, and support from my friends and family.

I would like to express my deepest gratitude to my advisor, Dr. Tzyy-Ping Jung, for his consistent support of my research. I would like to thank Dr. Gert Cauwenberghs for his guidance as the co-chair of my committee. I would also like to thank Dr. Silva, Dr. de Sa, and Dr. Cheng for their participation in my committee and providing valuable suggestions for my study.

I especially want to thank my colleagues, Yuan-Pin Lin and Yu-Te Wang, who were always helpful in my research and my life. I would also like to thank Dr. Makeig and all others in Swartz Center for Computational Neuroscience for their support and encouragement.

Finally, I would like to thank my parents and my elder brother for their great support and best wishes. My wife, Chun-Ju Chen, was always there stood by me through the hardest times. My daughter, Lyra Wei, was always cheering me up with her sweetest smile. This dissertation is dedicated to the endless love from my family.

Chapter 2 and 4, in part, contains materials from “Towards Plug-and-Play Brain State Decoding for Drowsiness with Large-Scale Data and Baseline Calibration ” by Chun-Shu Wei, Yuan-Pin Lin, Yu-Te Wang, Chin-Teng Lin, and Tzyy-Ping Jung, which was submitted to *NeuroImage* and is currently under a second revision. The dissertation author was the first author of the paper.

Chapter 3, in part, contains materials from “Toward Drowsiness Detection Using Non-Hair-Bearing EEG-Based Brain-Computer Interfaces” by Chun-Shu Wei, Yu-Te

Wang, Chin-Teng Lin, and Tzyy-Ping Jung, which has been submitted to *IEEE Transactions on Neural System and Rehabilitation* and is currently under review. The dissertation author was the first investigator and author of this paper.

Appendix A is largely a reprint of material from “Selective Transfer Learning for EEG-Based Drowsiness Detection” by Chun-Shu Wei, Yuan-Pin Lin, Yu-Te Wang, Tzyy-Ping Jung, Nima Bigdely-Shamlo, and Chin-Teng Lin, which appears in the *IEEE Conference on Systems, Man, and Cybernetics (SMC 2015)*. The dissertation author was the first investigator and author of this paper. The material is copyright ©2015 by the Institute of Electrical and Electronics Engineers (IEEE).

Appendix B is largely a reprint of material from “Exploring the EEG Correlates of Neurocognitive Lapse with Robust Principal Component Analysis” by Chun-Shu Wei, Yuan-Pin Lin, and Tzyy-Ping Jung, which appears in *the Proceedings of International Conference on Augmented Cognition, 2016*. The dissertation author was the first investigator and author of this paper. The material is copyright ©2016 by Springer International Publishing AG.

VITA

- 2009 Bachelor of Science, National Chiao Tung University, Taiwan.
- 2011 Master of Science, National Chiao Tung University, Taiwan
- 2017 Doctor of Philosophy, University of California San Diego, La Jolla.

PUBLICATIONS

Journal Article

- C.-S. Wei, Y.-P. Lin, Y.-T. Wang, C.-T. Lin, and T.-P. Jung, “Towards Plug-and-Play Brain-State Decoding with Large-Scale Data and Baseline Calibration,” *Neuroimage* (in revision)
- C.-S. Wei, Y.-T. Wang, C.-T. Lin, and T.-P. Jung, “Towards Drowsiness Detection using Non-Hair-Bearing EEG-Based Brain-Computer Interfaces”, *IEEE Transactions on Neural Systems and Rehabilitation Engineering* (in revision)
- Y.-T. Wang, M. Nakanishi, Y. Wang, C.-S. Wei, C.-K. Cheng, and T.-P. Jung, “An Online Brain-Computer Interface Based on SSVEPs Measured from Non-Hair-Bearing Areas,” *IEEE Transactions on Neural Systems and Rehabilitation Engineering*, 25(1), 14-21, 2017
- Y.-T. Wang, K.-C. Huang, C.-S. Wei, T.-Y. Huang, L.-W. Ko, C.-T. Lin, C.-K. Cheng, and T.-P. Jung, “Developing an EEG-Based On-Line Closed-Loop Lapse Detection and Mitigation System,” *Frontiers in Neuroscience*, 8, 2014
- Y.-P. Lin, Y. Wang, C.-S. Wei, and T.-P. Jung, “Assessing the Quality of Steady-State Visual-Evoked Potentials for Moving Humans using a Mobile Electroencephalogram Headset,” *Frontiers in Human Neuroscience*, 8, 2014.

Peer-reviewed Conference Paper

- C.-S. Wei, Y.-P. Lin, Y.-T. Wang, C.-T. Lin, and T.-P. Jung, “Transfer Learning with Large-Scale Data in Brain-Computer Interfaces,” *the 38th Annual International Conference of the IEEE Engineering in Medicine and Biology Society (EMBC’16), Orlando, USA, 2016.*
- C.-S. Wei, Y.-P. Lin, N. Bigdely-Shamlo, Y.-T. Wang, C.-T. Lin, and T.-P. Jung, “Selective Transfer Learning for EEG-Based Drowsiness Detection,” *IEEE International Conference on System, Man, and Cybernetics (SMC’15), Hong Kong, China, 2015.*
- C.-S. Wei, Y.-T. Wang, C.-T. Lin, and T.-P. Jung, “Toward Non-Hair-Bearing Brain-Computer Interfaces for Neurocognitive Lapse Detection,” *the 37th Annual International Conference of the IEEE Engineering in Medicine and Biology Society (EMBC’15), Milano, Italy, 2015.*
- C.-S. Wei, Y.-P. Lin, Y. Wang, Y.-T. Wang, and T.-P. Jung, “Detection of Steady-State Visual-Evoked Potential Using Differential Canonical Correlation Analysis,” *the 6th International IEEE/EMBS Conference on Neural Engineering (NER ‘13), San Diego, USA, 2013*
- C.-S. Wei, L.-W. Ko, S.-W. Chuang, T.-P. Jung, and C.-T. Lin, “Genetic Feature Selection in EEG-Based Motion Sickness Estimation,” *2011 International Joint Conference on Neural Networks (IJCNN ‘11), San Jose, California, USA, 2011.*
- C.-S. Wei, L.-W. Ko, S.-W. Chuang, T.-P. Jung, and C.-T. Lin, “Motion Sickness Estimation using an EEG-based Evaluation System,” *the 5th International IEEE EMBS Conference on Neural Engineering (NER ‘11), Cancun, Mexico, 2011.*

- C.-S. Wei, S.-W. Chuang, W.-R. Wang, L.-W. Ko, T.-P. Jung, and C.-T. Lin, “Implementation of a Motion Sickness Evaluation System Based on EEG Spectrum Analysis,” *the IEEE International Symposium on Circuits and Systems (ISCAS '11)*, Rio de Janeiro, Brazil, 2011.
- C.-S. Wei, C.-H. Tsai, S.-M. Chiou, Y.-T. Hseu, T.-W. Liu, H.-Y. Lai, T.-F. Chien, Y.-H. Kuo, W.-T. Zhao, Y.-S. Tang, S. Y. Su, and Y.-Y. Chen, “Nonlinear Analysis of Movement-related Changes in Human Subthalamic Local Field Potentials,” *the 32th Annual International Conference of the IEEE Engineering in Medicine and Biology Society (EMBC'10)*, Buenos Aires, Argentina, 2010.

Book Chapter

- C.-S. Wei, Y.-P. Lin, Y. Wang, and T.-P. Jung, “Exploring the EEG Correlates of Neurocognitive Lapse with Robust Principal Component Analysis,” *Human-Computer Interaction. Towards Intelligent and Implicit Interaction* (pp. 448-453). Springer Berlin Heidelberg, 2016.
- Y.-P. Lin, Y. Wang, C.-S. Wei, and T.-P. Jung, “A mobile brain-computer interface for freely moving humans,” *Human-Computer Interaction. Towards Intelligent and Implicit Interaction* (pp. 448-453). Springer Berlin Heidelberg, 2013.
- L.-W. Ko, C.-S. Wei, T.-P. Jung, and C.-T. Lin, “Estimating the Level of Motion Sickness Based on EEG Spectra,” *Foundations of Augmented Cognition. Directing the Future of Adaptive Systems* (pp. 169-176). Springer Berlin Heidelberg, 2011.

ABSTRACT OF THE DISSERTATION

Towards Brain Decoding for Real-World Drowsiness Detection

by

Chun-Shu Wei

Doctor of Philosophy in Bioengineering

University of California, San Diego, 2017

Professor Tzyy-Ping Jung, Chair
Professor Gert Cauwenberghs, Co-Chair

A brain-computer interface (BCI) allows humans to communicate with a computer by thoughts. Recent advances in brain decoding have shown the capability of BCIs in monitoring physiological and cognitive states of the brain, including drowsiness. Since drowsy driving has been an urgent issue in vehicle safety that causes numerous deaths and injuries, BCIs based on non-invasive electroencephalogram (EEG) are developed to monitor drivers' drowsiness continuously and instantaneously. Nonetheless, on the pathway of transitioning laboratory-oriented BCI into real-world applications, there are major challenges that limit the usability and convenience for drowsiness detection (DD).

To completely understand the association between human EEG and drowsiness, this study employed a large-scale dataset collected from simulated driving experiments with a lane-keeping task and EEG recordings. A drowsiness index based on response time data was proposed to capture the fluctuations in drowsiness level during driving sessions. Multi-channel EEG spectral powers were extracted and related to the drowsiness index within sessions for multiple subjects. Hierarchical clustering analysis was applied to the EEG-drowsiness correlations across sessions and across features, providing the following insights: 1) Similar EEG-drowsiness correlations are found among different subjects. 2) EEG features are reducible in the channel (spatial) domain.

Current DD-BCIs are facilitated with wet or dry electrodes deployed across the whole scalp. The usage of wet electrodes involves head washing due to the use of conductance gel, and the pin-shaped dry electrodes for hair-cover areas result in erythema after sustained use. A DD-BCI that acquires EEG from only non-hair-bearing (NHB) areas was proposed to maximize comfort and convenience. The performance of the NHB DD-BCI was validated and compared with that using whole-scalp EEG, showing no significant difference in the accuracy of alert/drowsy classification.

In addition, the issue of human variability in brain dynamics was addressed. Inter- and intra-subject variabilities limit the reproducibility of brain responses across time and across individuals, resulting in a time-consuming calibration before each use of a BCI. In particular, drowsiness-related EEG data are difficult to obtain, since drowsiness is not immediately inducible for a new user. Therefore, a subject-transfer framework that leverages large-scale existing data from other subjects was proposed to reduce the calibration time of a DD-BCI. Alert baseline data were involved to enhance the efficiency

of subject-to-subject model transfer. Data size positively impacted the performance of the proposed subject-transfer approach, and the alert baseline data were shown effective in estimating subject similarity in drowsiness-related brain responses. The subject-transfer approach significantly reduced the calibration time of the DD-BCI, exhibiting the potential in facilitating plug-and-play brain decoding for real-world BCI applications.

Overall, this thesis presents the contributions to developing a DD-BCI for real-world use with maximal usability and convenience. The methodologies and findings could further catalyze the exploration of real-world BCIs in more applications.

CHAPTER 1

INTRODUCTION

Reading minds has been a fascinating topic in science and engineering. To translate brain activities into messages to an external device or a computer, a brain-computer interface (BCI) that senses brain activity and recognizes the underlying patterns is required to facilitate the brain-computer interactions [1][2][3]. Brain activities can be obtained by numerous neuromonitoring modalities that vary in temporal resolution, spatial resolution, invasiveness, and cost [4][5][6]. Among those modalities, electroencephalogram (EEG) is the most common in developing real-world BCI applications, as EEG is non-invasive, affordable, and with high temporal resolution. A BCI that is capable of real-world use is supposed to have the following characteristics:

(A) Robustness.

The accuracy of pattern recognition is maintained at an acceptable level across long-term use regardless of the user.

(B) Convenience.

The wearable device needs to be wireless, portable, easy to setup, and comfortable for sustained use. The initiation of the BCI system should be rapid without time-consuming calibration.

(C) Affordability.

The cost of hardware and software included in the BCI system is supposed to be affordable or at least lower than the benefit produced.

BCIs based on EEG have been used for a number of purposes including sending text messages and controlling moving objects by thoughts. BCI spellers have been designed using an event-related potential, P300, to generate commands for typing letters, number, and symbols [7]. Another type of BCI spellers based on steady-state evoked potential (SSVEP) can achieve a higher information transfer rate using flickering visual stimuli coded in a range of frequencies and phases [8]. On the other hand, motor-imagery brain responses are used in BCIs for controlling moving objects intuitively. Motor-imagery BCIs have been applied to controlling computer cursors [9], wheelchairs [10], and quadcopter drones [11]. Lower extremity prostheses controlled by a motor-imagery BCI were demonstrated to allow a patient with spinal cord injury (SCI) to walk [12]. The integrated framework that combines prostheses with BCI control has been shown to improve the walking performance of SCI patients through neurological recovery triggered by BCI usage [13]. Furthermore, recent advances in brain decoding based on EEG have shown potential in monitoring brain states associated with physiological or cognitive status. In clinical applications, EEG has been used to monitor the depth of coma, anaesthesia, sleep, and the occurrence of epilepsy [14]. Lately, EEG-based BCI is proposed to detect drivers' drowsiness in order to prevent drowsy driving, an urgent issue in vehicle safety. According to the statistics, drowsy driving caused 37,000 injury crashes, resulting in 886 fatal crashes at the year of 2014 [15]. A BCI system for drowsiness detection (DD) usually consists of the following components,

(A) *Signal acquisition.*

A non-invasive EEG device is applied to record EEG signals continuously from the scalp regions of interest and convert the analog signals into digital samples.

(B) Signal processing.

Raw digital signals from multi-channel EEG recording are further processed with a series of procedures including down-sampling, referencing, filtering, and data cleaning.

(C) Feature extraction.

Informative features related to drowsiness are extracted from the clean data.

(D) Pattern recognition.

The drowsiness-related patterns within the EEG features are recognized by a pattern recognition model. The model inputs EEG features and outputs a predicted drowsiness level. Machine learning techniques might be needed for training the model to detect drowsiness.

(E) Feedback.

The output of the DD model can be used to manage drowsiness in various forms of intervention such as arousal feedbacks.

The associations between EEG and drowsiness have been explored in numerous studies for more than two decades. EEG spectral powers were first investigated in the experiments where sustained attention tasks were performed [16][17][18], where positive correlations were found at the theta (4-8 Hz)/alpha (8-13 Hz) band at multiple brain regions. Exploiting the EEG-drowsiness associations, Lin et al. [19] proposed a drowsiness-estimation system that predicts driving error using 32-channel EEG spectral powers with a linear regression model. The model was trained using a pilot session and tested on the next session of the same individual. Later on, Davidson et al. [20]

demonstrated a subject-independent approach to detect drowsiness with 16-channel EEG band powers. Although these works did not validate the online performance of their DD-BCIs, their results suggest the potential of EEG-based DD in monitoring the emergence of drowsiness continuously and instantaneously.

Despite these advances that show the feasibility of a DD-BCI, more implementation considerations emerge in the transition from a well-controlled laboratory to a variable real-world environment. One grand challenge in real-world DD-BCI is the lack of convenience of EEG-based brain monitoring, the current modality. In most of the current BCIs, EEG signals are acquired from wet or dry electrodes deployed on the scalp. To establish a stable contact between electrodes and skin, wet electrodes require conductive gel to minimize the electrode-skin impedance. The preparation could be time-consuming depending on the density of electrodes. Also, hair washing after use causes severe inconvenience. Meanwhile, EEG devices based on dry electrodes without conductive gel can be set up easily and quickly with satisfactory signal quality [21][22][23]. However, the pin-shaped design of dry electrodes for penetrating the hair layer could cause erythema after long-term use [24]. Another problem within the current DD-BCI modality is the whole-scalp EEG recording that results in a bulky wearable device on top of the scalp, regardless of the usage of wet or dry electrodes. All of the above-mentioned issues motivate us to design a novel EEG recording montage that is applied only to non-hair-bearing (NHB) areas, including frontal and mastoid areas. One advantage of the NHB montage is the reduction of the recording area that could minimize the size and weight of an EEG device. In addition, without the interference of the hair layer, gel-based wet electrodes and pin-shaped dry electrodes are no longer needed. In the

NHB areas, newly developed deformable patch sensors or tattoo sensors are available with maximal comfort for long-term use [25][26]. The major concern of using NHB EEG-based BCI is the difficulty of accessing the signal of interest, since NHB areas cover limited peripheral areas. Therefore, it is imperative to explore the efficacy of NHB EEG in the associations with drowsiness and in the decoding performance compared with whole-scalp EEG.

Another challenge in applying DD-BCI in the real world comes from the pervasive and elusive human variability in brain dynamics. Each person has a unique brain [27], and the variance among individuals is termed inter-subject variability. Within the same individual the brain, as a dynamic system, could work differently across time [28][29], causing session-to-session or intra-subject variability. The inter- and intra-subject variabilities jointly limit the reproducibility of specific brain responses, and thus constrain the generalizability of brain decoding algorithms. To deal with inter- and intra-subject variabilities, conventional BCI design incorporates a calibration session to collect sufficient training data for building a brain-decoding model for a single user, and the model is usually used specifically for the immediately upcoming executing session to minimize intra-subject variability [1][3]. This self-decoding approach that utilizes the calibration data within the same subject has been the standard for constructing a BCI decoding model. However, the conventional calibration could be time-consuming depending on the amount of data required that supports the robustness of the brain decoding model. In practical applications of BCIs, laborious calibration becomes an inevitable obstruction in terms of convenience and usability. Particularly for a DD-BCI, EEG data in the drowsy state is much more difficult to obtain than in the alert state.

Subject-independent approaches have been proposed to exploit robust feature-extraction methods that are insensitive to inter-subject variability [30][31][32][33]. Nonetheless, loss in decoding performance of using subject-independent approaches is inevitable, compared to using subject-dependent approaches that include individualized data [30][31]. On the other hand, there are subject-dependent approaches that utilize data from other subjects and from the new user as well. Those approaches use a small amount of individualized data from the new user to facilitate the subject-to-subject transfer of decoding models with less loss in performance. Since these subject-transfer schemes might be comparable to conventional self-decoding approach in decoding performance, these methods are applied to reduce calibration time for a new BCI user. Either subject-independent or subject-dependent approaches rely on data from other subjects, and data sufficiency is critical to their performances [34]. Nonetheless, as mentioned earlier, data collection in the drowsy or certain other brain states is arduous due to the uncertainty of inducing the brain state. Even a small amount of drowsiness-related EEG data might not be instantly available from a new user.

While collecting drowsiness-related data could be time-consuming and expensive, non-drowsy data such as baseline EEG activity in the alert state might be useful in tackling inter-subject variability. The alert baseline EEG activity can be easily obtained from an alert resting state when subject is not engaged in a specific task. Studies have shown the associations between task-relevant and task-free brain activity in terms of the patterns of functional connectivity [35][36]. The alert baseline EEG activity of multiple subjects might carry information of how similar these subjects' drowsiness-related brain responses are. If this assumption holds, the alert baseline data can be utilized to identify

the similarity among subjects, and thus enhance the efficiency of a subject-transfer framework. In this framework, large-scale existing data from multiple subjects with diversity might be important for supporting positive data/model transfer.

This thesis summarizes the effort that has been made for facilitating the use of a DD-BCI in a real-world application. The contributions comprise three main significances: 1) analysis on EEG-Drowsiness associations using a large-scale datasets 2) NHB montage for light and comfort EEG monitoring and 3) a subject-transfer framework for a plug-and-play DD-BCI. The constitutive principle and rationale of the methodologies are addressed in detail, and the results are exhibited with discussions on the impact of the findings. The main text of this thesis is organized along the following thematic lines.

Chapter 2 describes a series of data analyses performed on a large-scale EEG dataset of drowsiness. A drowsiness index was proposed to estimate the drowsiness level during driving and investigate its association with EEG features. Based on the individual pattern of EEG-drowsiness correlations, hierarchical clustering was applied to visualize the data similarity and variability among sessions/subjects and among EEG features. The insights gained from these analyses elicited essential traits of drowsiness-related brain dynamics and fertilized solving strategies for the real-world problems.

Chapter 3 addresses an important issue on the convenience of BCIs in real-world environment in terms of EEG acquisition. A DD-BCI was proposed featuring the application of NHB EEG signals. The drowsiness-related brain response observed from hair-cover areas and NHB areas were quantitatively investigated, and a comparison was made between the performances obtained using the NHB DD-BCI and the conventional whole-scalp montage.

Chapter 4 exhibits a study that aimed to minimize calibration time of a DD-BCI using large-scale data and baseline calibration. A comprehensive review of subject-transfer approaches for calibration time reduction in BCI studies is provided. A subject-transfer framework was proposed to obviate conventional individualized task-relevant calibration. A large-scale dataset was exploited to ensure the size and diversity of a source data pool, and baseline calibration was employed to estimate the subject similarity in drowsiness-related brain dynamics.

Chapter 6 summarizes the contributions of this dissertation and discusses possible future research directions.

CHAPTER 2

ASSOCIATIONS BETWEEN EEG DYNAMICS AND DROWSINESS AND THEIR VARIABILITY ACROSS SUBJECTS AND SESSIONS

This chapter describes the study for completely understanding the association between human EEG and drowsiness based on a large-scale dataset collected from simulated driving experiments with a lane-keeping task and EEG recordings. A drowsiness index based on response time data was proposed to capture the fluctuation of drowsiness level across a driving session. Multi-channel EEG spectral powers were extracted and related to the drowsiness index within a session for multiple subjects. Hierarchical cluster analysis was applied to the EEG-drowsiness correlations across sessions and across features, providing the following insights: 1) Similar EEG-drowsiness correlations are found among different subjects, and 2) EEG features are reducible in channel (spatial) domain.

2.1 Background

Drowsiness is one of the major causes of fatal accidents in vehicle driving. According to the statistics assessed by the U.S. Department of Transportation National

highway Traffic Safety Administration, drowsy driving caused 37,000 injury crashes resulting 886 fatal crashes at the year of 2014 [15]. It is a high-priority issue in life safety, and requires development in science and technology that enables real-time drowsiness detection. For the past two decades, non-invasive brain-sensing technology such as electroencephalogram (EEG) has shown promising capability in tracking human cognitive state as it features high temporal resolution, excellent portability, and affordable cost among current brain monitoring modalities [4][5][6].

The association between EEG and drowsiness has been revealed by investigating the change of EEG features in a sustained-attention task that requires a human subject to focus on specific stimuli and make response instantaneously. The most commonly used EEG features related to drowsiness are the spectral powers at different frequency bands [17][18][19][37]. Jung et al. [17] extracted the fluctuation in EEG spectra in an auditory monitoring task and EEG spectra and found high positive correlation between the powers around theta (4-8 Hz) band present and the task error. Parikh et al. [18] and Lin et al. [19] show positive correlation between EEG alpha (8-13 Hz) power and task performance in simulated driving experiments. The discrepancy might be resulted from the pervasive and elusive variability in human brain dynamics.

In this study, we employed a large-scale dataset including human behavior and EEG data from a driving experiment with a lane-keeping task. We aimed to analyze and summarize the spatio-temporal relationship between EEG spectral powers and drowsiness level. Furthermore, we applied hierarchical cluster analysis to the EEG-drowsiness correlations to investigate the data similarity among EEG features and the variability among sessions and individuals.

2.2 Materials and Methods

A lane-keep driving experiment was employed in this study to investigate the brain dynamics associated with human performance in a sustained-attention driving task [38]. The driving experiment was performed in a realistic virtual-reality (VR) driving simulator that utilized a real car cabin mounted on a 6-degree-of-freedom motion platform with surrounding projector screens displaying the driving scene [21][39]. The driving scene was on a nighttime straight highway with a constant cruising speed of 100 km/h (computer controlled), and only wheel-steering control was required from the subject. In this lane-keeping task (LKT), lane-departure events were randomly introduced during cruising, which made the car drifted toward left or right. The participants were instructed to steer the car back to the original cruising lane as quickly as possible, and the initiation of participants' movements terminated the voluntary drifting of the car. After the car was back to the course and continued cruising, the next lane-departure event occurred within an inter-trial interval of 6-10 seconds. The paradigm of the lane-keeping driving task is illustrated in Figure 2.1 Time points corresponding to the occurrences of lane-departure events, subject's movements responding to the lane-departure events, and completions of wheel steering were logged as deviation onsets, response onsets, and response offsets, respectively. For each trial, response time (RT) was measured from the deviation onset to the response onset, which served as a behavioral assessment of drowsiness in the lane-keeping task. The experiment was performed after lunch, and lasted for ~90 minutes to maximize the chance of drowsy driving and to accumulate sufficient trials within a session.

Thirty-seven healthy volunteer subjects with normal or corrected-to-normal vision participated in the experiment, and in total performed 79 sessions of the lane-keeping driving task. Part of the dataset has been exploited to conduct several previous studies [19][40][41][42]. Of all the subjects, thirteen of them contributed a single session, and 24 of them performed multiple sessions (2 - 5) on different days. Each subject was in normal circadian rhythm and had sufficient sleep before performing the experiment. The Institutional Review Board of the Veterans General Hospital, Taipei, Taiwan approved this experimental protocol. All the subjects were asked to read and sign an informed consent form before performing the experiments.

2.2.1 Behavioral Analysis

In this study, the level of drowsiness in the lane-keeping task refers to momentary unresponsiveness to the lane-departure event, and was quantitatively assessed based on the RT following each deviation onset. To build a predictive model for decoding alert/drowsy state, it is required to have sufficient fluctuations in the RTs within a session for accumulating an adequate amount of data from the alert/drowsy state. A session with the desired driving behaviors was defined with the following criteria: 1) accumulation of at least 100 trials, 2) a baseline in the alert state, i.e., accumulation of at least 10 alert trials at the beginning of the session, and 3) accumulation of at least 10 drowsy trials. The trials with RTs less than $1.5 \times \tau_0$ were categorized as ‘alert’ trials, where τ_0 denotes the alert RT estimated by the median of the RTs of the first 10 trials (all alert trials) in a driving session [43]. On the other hand, the drowsy trials were those with RTs larger than $2.5 \times \tau_0$. Because τ_0 was obtained by session-wise estimation, it could account for the variation of the RTs to lane-departure events in the alert state across different sessions

and subjects. If a subject has a longer alert RT, then the threshold of drowsy RT is inherently higher for the subject. Based on the requirements, fifty-four sessions from 25 subjects that showed desired driving behaviors were selected for further analysis in this study. Among the 25 selected subjects, eight subjects performed a single session, and 17 subjects performed multiple (2-5) sessions.

We have formerly proposed a normalized index for mapping the semi-infinite RT distribution to a bounded measurement, named drowsiness index (DI), ranging from 0 to 1, which takes the individual difference in the RT of the alert state (alert RT) into account (Wei et al., 2016) [43]. The following formula was utilized to convert the RT into the DI at the moment of a given lane-departure event:

$$DI = \max(0, (1 - e^{-a(\tau - \tau_0)}) / (1 + e^{-a(\tau - \tau_0)}))$$

where τ is the RT of the given lane-departure event, and a is a constant set as 1 s^{-1} . In practice, the DI requires further smoothing using a causal 90-s uniform moving-average filter to eliminate short-term variation that might not be attributed by drowsiness (Jung et al., 1997). Finally, we employed the smoothed DI as the response variable in the regression analysis.

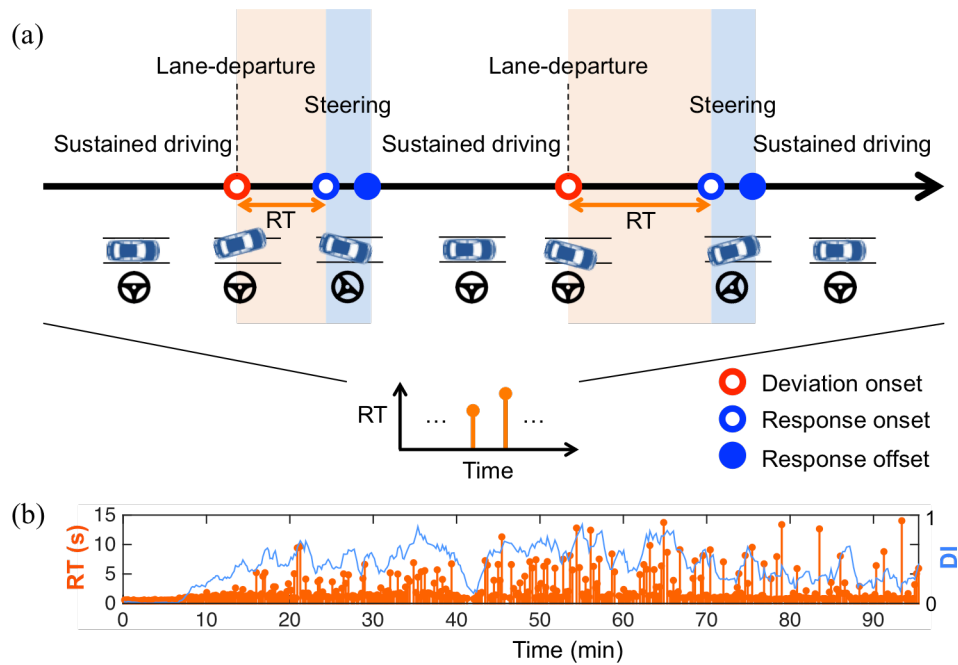


Figure. 2.1: (a) The experimental paradigm of the lane-keeping driving task. Lane-departure events were introduced once per trial every 6-10 s in the sustained driving. For each trial, the occurrences of lane-departure events, the initiation of subject's movements responding to the lane-departure events, and the completions of wheel steering were logged as the deviation onsets, response onsets, and response offsets. The RT of a given trial was measured according to the duration between the deviation onset and the response onset; (b) Change of the RT and the RT-based DI across a sample session (S41-4). The RTs across the session are marked by the orange stems. The DI is illustrated as the blue curve.

2.2.2 EEG Recording and Processing

The EEG data were recorded by a 32-channel Quik-Cap electrode system (Compumedics Neuroscan, Inc.). Thirty Ag/AgCl electrodes were deployed according to a modified International 10-20 system, referencing to two reference electrodes located upon left and right mastoid areas. The impedance of Ag/AgCl electrodes was maintained below 5k Ohm, and the skins under the reference electrodes were cleaned and abraded. The EEG signals were sampled with 16-bit quantization and 500-Hz sampling rate. The raw EEG data were then processed with a band-pass finite impulse response filter (2 to 30

Hz) to eliminate DC drift and high-frequency noise including 60 Hz power-line noise. Next, the filtered 30-channel EEG data were down-sampled to 250 Hz to reduce computational load for further analysis. Next, the high-variance artifacts in the signals, such as eye movement, blinking, muscle activity, and environmental noise, were removed using artifact subspace reconstruction (ASR) [44] provided in the EEGLAB toolbox [45]. Hereby the threshold of ASR was set at 10 times of standard deviation.

2.2.3 EEG Feature Extraction

Previous studies (Jung et al., 1997; Lin et al., 2005) [17][19] have reported significant EEG spectral correlates of RT in stereotype frequency bands, such as delta (2-5 Hz), theta (5-8 Hz), alpha (8-13 Hz), and beta (13-30 Hz) band. We first applied sub-band-pass filters to extract EEG signals in the delta, theta, alpha, and beta bands, and then calculated the band power (logarithmic signal variance) of each channel within a 3s window before the onsets of lane-deviation events and at least 3s after the offsets of wheel-steering movements of the previous trials (Wei et al., 2016) [43]. The 3s time window before the lane-deviation event refers to the inter-trial cruise-driving period, and was used for extracting EEG power features that were not evoked or elicited by lane-deviation events, subject responses, or kinesthetic feedback. The cruise-driving EEG power of each trial was later averaged with the EEG powers of previous adjacent trials within 90 seconds to generate the smoothed cruise-driving EEG power (in accordance with the smoothed DI) that carried less irrelevant spectral perturbation compared to the unsmoothed power. Finally, the smoothed multi-channel EEG powers formed a 120-dimensional (4 frequency bands \times 30 channels) feature space.

2.2.4 Hierarchical Cluster Analysis

Hierarchical cluster analysis (HCA) has been widely used in recent scientific research for extracting and visualizing characteristics in a large-scale dataset efficiently. Particularly in the field of bioinformatics, HCA is commonly used jointly with a heat map of gene expressions to explore the patterns and linkages across numbers of genes and experimental measurements [46]. This study extends the utility of HCA to explore the underlying traits of a multi-subject EEG dataset.

Through the above-mentioned feature extraction, a heat map was then constructed based on the correlation coefficients between the EEG spectral features and the DI fluctuations. The 2-dimensional heat map has one dimension (row) across sessions from multiple subjects, and the other dimension (column) across the EEG spectral features across channels and frequency bands. The HCA was applied to both dimensions of the map, presenting the session-wise and feature-wise similarity/variability in the dataset. The clustering linkages among features (columns) present the relationship of EEG dynamics across channels and frequency bands in terms of their similarities across multiple sessions/subjects. On the other hand, the clustering linkages among sessions exhibit the reproducibility of the EEG dynamics with the same or across different subjects [17], i.e., the intra- and inter-subject variabilities of the drowsiness-related brain responses across spatial and spectral domain. The intra- and inter-subject variabilities revealed in the HCA examine the feasibility of using subject-transfer approach for decoding the specific brain activity. When a large intra-subject variability is shown, transferring brain-decoding models from other subjects might result in a comparable (or

even better) decoding performance than training a model with other sessions from the same subject.

2.3 Results

This section describes the results obtained from basic data analysis and hierarchical clustering. We first analyzed and visualized EEG correlates of drowsiness in terms of spatial distributions of EEG spectra and EEG-DI correlations as shown in Figure 2.2. The EEG-DI correlations for a single session (S41-4, Figure 2.2(a)) appear to be positive in the delta and theta bands, and negative in the alpha and beta bands. Figure 2.2(b) shows scatter plots of EEG power and smoothed DI at the representative channels along the midline using all the trials in the session.

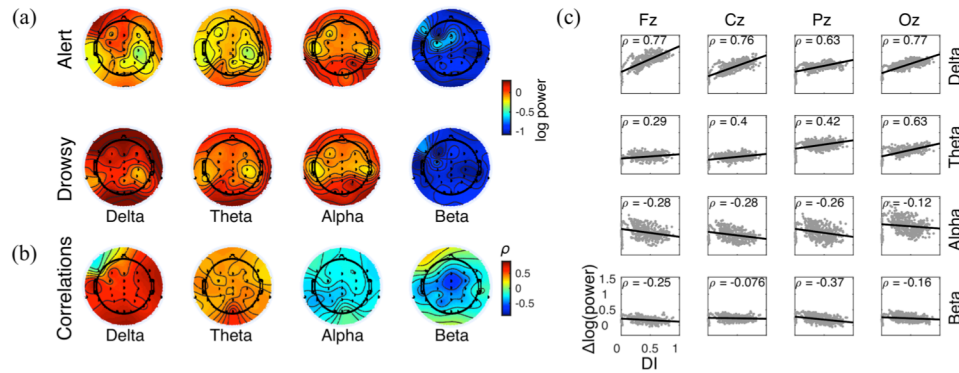


Figure. 2.2: (a) Topography of spatial distributions of EEG band powers in the alert and drowsy states; (b) EEG-DI correlation of a sample session (S41-4); (c) Scatter plots of EEG band powers against DI at representative channels along the midline, Fz, Cz, Pz, and Oz. Correlation coefficients are denoted at the upper-left corner, and linear fittings are shown as black lines.

Figure 2.3 shows the topography of the EEG-DI correlations in two sessions from the same subject (S5) on different days. The first session exhibited strong positive EEG-DI correlations in the theta, alpha, and beta bands, but these correlates were not

reproduced in the second session, where a strong positive correlation in the delta band and a negative correlation in the alpha powers were exhibited.

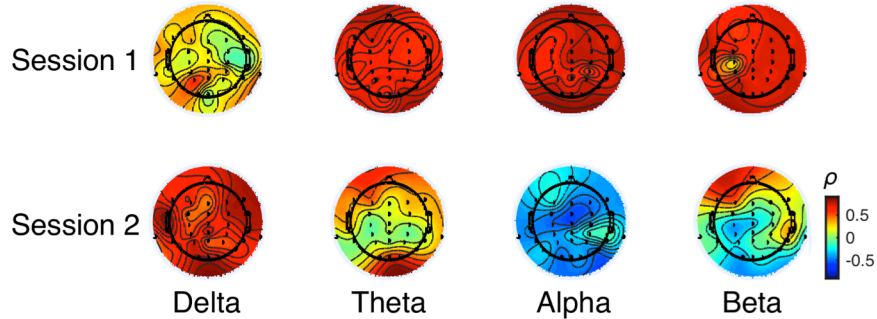


Figure. 2.3: The topography of EEG-DI correlations in sessions S5-1 and S5-2. Drastic discrepancy appears in the EEG-DI correlations in the alpha band (a strong positive correlation across the whole scalp in session 1 versus a strong negative correlation in session 2 from the same subject).

To investigate the variability of drowsiness-related EEG dynamics across multiple subjects, we constructed a heat map to illustrate the EEG-DI correlation across all EEG features (4 frequency bands \times 30 channels) and all sessions from different subjects (see Figure 2.4). HCA was applied to both dimensions of the heat map to assess the inter- and intra-subject variabilities of drowsiness-related brain dynamics (along rows), and the similarity among EEG features (along columns) with average-linkage dendrograms. Along the columns, the clustering of EEG features formed several large high-level groups based on the frequency bands, and adjacent channel locations in the same frequency bands were linked within the low-level groups of frequency bands.

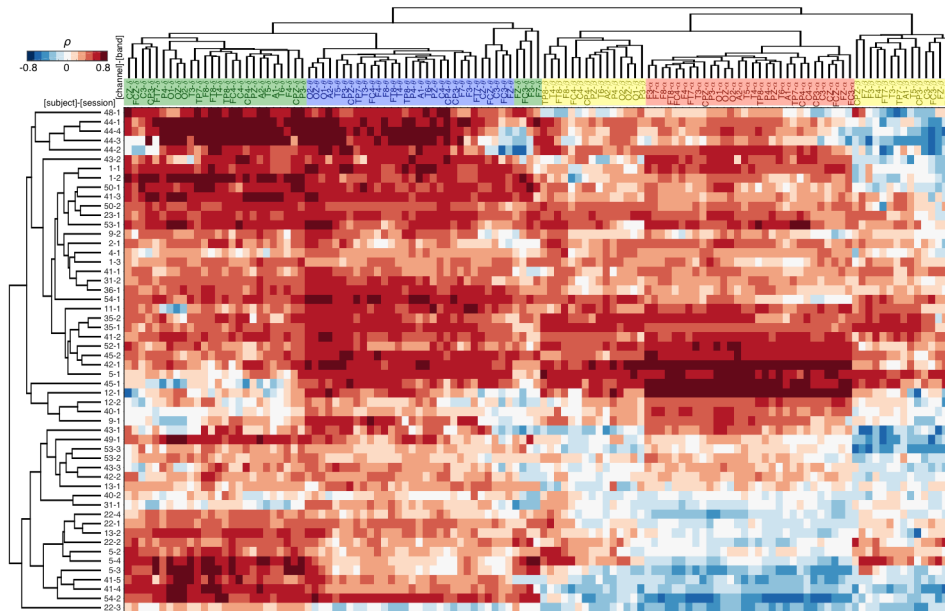


Figure. 2.4: Hierarchically clustered sessions (rows) and EEG power features (columns) with dendrograms across 54 sessions from 25 subjects who experienced drowsiness in the LKT experiments. Red/blue pixels in the heat map indicate positive/negative correlations between the logarithmic EEG band powers (4 frequency bands \times 30 channels) and the change of DI measured by the RT in the LKT. For explicitness, the labels of EEG power features were highlighted with different colors for different frequency bands (δ : green; θ : blue; α : red; β : yellow). Note that, either within- or cross-subject sessions are grouped together, suggesting these sessions share common brain responses of spectral change associated with drowsiness. As different subjects exhibited similar EEG-DI correlations, their models for drowsiness detection could be transferred among each other.

Meanwhile, along the rows, the inter- and intra-subject variabilities are indicated by the links among sessions. For some subjects such as S44, four sessions from the subject were grouped together, indicating small intra-subject variability. Other subjects, however, had high intra-subject variability in EEI-DI correlations across sessions, as evidenced by the separation of their within-subject sessions in the dendrogram. In sum, the binding of sessions within the same subject occurred in only 6 out of 17 subjects who performed multiple sessions. It is worth noting that contradictory EEG-DI associations could be found in sessions from the same subject (e.g. S41- $\{1, 2, 3\}$ vs S41- $\{4, 5\}$ in the alpha band). This finding emphasizes that models across different subjects can be used to

obviate the intra-subject variability that deteriorates the performance of conventional brain-decoding schemes.

The pairing between different subjects suggests the feasibility of subject-to-subject transfer of source models, since analogous EEG-DI associations could be found in the data from other subjects within a group or adjacent groups. Nonetheless, the patterns shown in the heat map reveal the possibility of negative transferring when a source model is transferred to a dissimilar subject. For example, some EEG features (e.g. alpha power) showed positive correlations (red) with drowsiness for some subjects (e.g. Subject 12-1) but showed negative correlations (blue) for others (e.g. Subject 54-2). Therefore, a method to identify similar (supportive) sessions/subjects and to exclude dissimilar sessions/subjects is imperative for the subject-transfer approaches.

2.4 Discussion

The intra- and inter-subject variabilities in EEG have hindered the developments and applications of brain decoding systems. Such intra-subject variability may source from changes in neural processing [47], non-stationarity of EEG [48], and numerous neurophysiological mechanisms [49]. As shown in Figure 2.3, strong positive EEG-DI correlations in the theta and beta bands, which were prominent in the first session, diminished in the second session. This inconsistency in EEG-DI correlation across sessions indicates the day-to-day intra-subject variability of brain dynamics associated with drowsiness. To explicitly illustrate the variability in the EEG dynamics across multiple sessions and subjects, we applied HCA to the large-scale EEG dataset, and investigated the cross-session and the cross-feature relationships of the drowsiness-

related brain activity. As shown in Figure 2.4, theta band power had the most consistent EEG-DI associations across subjects, which is in line with previous studies that reported strong drowsiness associations in the theta band [17][50]. The clustering across sessions and subjects resulted mostly in cross-subject pairs and groups. Meanwhile, the multiple sessions from the same individual were separated and grouped with sessions from other subjects because of noticeable intra-subject variability. These linkages of EEG-DI associations across different subjects validate the feasibility of subject-to-subject model transferring among adjacent (supportive) subjects. In addition, the HCA in the EEG-DI correlations along the EEG features illustrates the similarity across channels and the variability across frequency bands. The clustering of the features suggests a larger similarity across different EEG channels (spatial domain) within a frequency band than that across different frequency bands (spectral domain). This reveals the dimensional redundancy in multi-channel EEG, which is well known to be a result of low spatial resolution in scalp EEG recordings. For the sake of channel selection and reduction, the consistency across different scalp channels implies the feasibility of using data from a small number of EEG channels to extract drowsiness-related brain response.

2.5 Conclusion

A novel scheme with hierarchical cluster analysis was proposed to gain a thorough understanding of the EEG-drowsiness associations. The correlations between EEG features and a RT-based DI were visualized in the hierarchical cluster analysis, where similar EEG-drowsiness correlations are found among different subjects. This finding suggests the feasibility of transferring decoding model across subjects.

Meanwhile, the EEG features appear similar and redundant across channels in spatial domain. Therefore, it might be possible to reduce the number of channels for EEG recording without loss in the decoding performance.

Acknowledgements

This chapter contains material partly from “Towards Plug-and-Play Brain State Decoding for Drowsiness with Large-Scale Data and Baseline Calibration ” by Chun-Shu Wei, Yuan-Pin Lin, Yu-Te Wang, Chin-Teng Lin, and Tzyy-Ping Jung, which has been submitted to *NeuroImage* and is currently under review. The dissertation author was the first investigator and author of this paper.

CHAPTER 3

DROWSINESS DETECTION USING NON-HAIR-BEARING EEG-BASED BRAIN-COMPUTER INTERFACES

Drowsy driving is one of the major causes that lead to fatal accidents worldwide. For the past two decades, many studies have explored the feasibility and practicality of drowsiness detection using EEG-based BCI systems. However, on the pathway of transitioning laboratory-oriented BCI into real-world environments, one chief challenge is to obtain high-quality EEG with convenience and long-term wearing comfort. Recently, acquiring EEG from NHB scalp areas has been proposed as an alternative solution to avoid many of the technical limitations resulted from the interference of hair between electrodes and the skin. Furthermore, our pilot study has shown that informative drowsiness-related EEG features are accessible from the NHB areas. This study extends the previous work to quantitatively evaluate the performance of drowsiness detection using cross-session validation with widely studied machine-learning classifiers. The offline results showed no significant difference between the accuracy of drowsiness detection using the NHB EEG and the whole-scalp EEG across all subjects ($p=0.31$). The findings of this study demonstrate the efficacy and practicality of the NHB EEG for

drowsiness detection, and could catalyze further explorations and developments of many other real-world BCI applications.

3.1 BACKGROUND

Drowsy driving is one of the major factors that lead to collisions, injuries, or even fatalities (NHTSA) [15]. Developing reliable approaches to detect drowsiness during driving is one of the high priority issues for life safety. For the past two decades, many studies have explored the feasibility and practicality of drowsiness detection using EEG, the most practical non-invasive modality featuring high temporal resolution and low cost among various types of brain monitoring modalities [2]–[7] (Makeig1993; Jung1997; Parikh 2004; Lin2005; Johnson2011; Chuang2014) [16][17][18][19][41][51]. In 1993, Makeig and Inlow [16] have investigated and quantified the correlation between EEG features and task performance (the error rate of detecting above-threshold auditory target stimuli). Subsequent work by Jung et al. demonstrated the feasibility of estimating alertness based solely on the variations of EEG spectral power in an auditory monitoring task (Jung1997) [17]. They proposed to build a predictive model using the EEG data collected in a training session, and then applied the model to the EEG recorded in a testing session from the same participant to continuously estimate the alertness level.

Based on the correlation between EEG spectra and drowsiness, several studies have contributed to developing algorithms that can estimate the performance of sustained-attention tasks [4]–[7] (Parikh2004; Lin2005; Joh) [18][19][51], which have solidified the practicality of a brain-computer interface (BCI) that tracks neurocognitive drowsiness continuously. Although the aforementioned studies have demonstrated the

detectability of drowsiness-related EEG markers, their results were obtained with whole-scalp EEG systems in well-controlled laboratory environments. Whether or not the EEG-based drowsiness detection method is practical in real-world environments remains unclear. Applying EEG measurements for monitoring changes of brain cognitive states has been known as one of the grand challenges because of various limitations existing in current EEG recording modalities [52][53]. In general, EEG acquisition for real-world applications requires following features [54][55]: 1) Portability, 2) Convenience and long-term wearing comfort, and 3) Acceptable signal quality. The conventional laboratory-oriented EEG recording methodology failed to meet aforementioned requirements because of the use of wet electrodes and conductive gels for reducing the impedance and tethered wires for connecting the computer systems. Furthermore, skin/scalp preparation and cleaning are both time-consuming and inconvenient before and after each EEG recording session. The recent advance in developing portable and wireless EEG recording devices has made significant improvements in terms of portability and convenience of EEG [12]–[14] (Chi 2012; Lin 2011; Grozea 2011) [56][57][58]. Nonetheless, dry-electrodes still face difficulty in achieving stable electrode-skin contact in hair-covered scalp areas without conductive gels. To reduce the interference from the hair between electrodes and the skin, current dry electrodes often used pins, either solid or flexible, to penetrate the hair layer [56][57][58]. According to a previous study on user experience of dry electrodes, even soft- pin-based electrodes could cause erythema after long-term applications [24]. Overall, in terms of portability, convenience, long-term wearing comfort, and acceptable signal quality, none of the existing EEG recording devices has met all of the requirements for real-world use.

However, even though the EEG recording devices might not have a satisfactory solution for real-world use immediately, there might be a compromise solution. Lately, a NHB montage that measures EEG signals from frontal, ear, mastoid, and neck areas has been proposed for measuring EEG signals in real-world BCI applications, because it avoids the interference of electrode-skin contact caused by the hair [26][59][60][61][62]. Generally speaking, the NHB BCI uses only easily assessable areas of the scalp, and could be realized with EEG recording devices featuring minimal weight and size, which are necessary for portability, convenience of use and long-term wearing comfort. Furthermore, without the interference from the hair, the relatively stable skin-electrode contact could improve the convenience of recording setup without the use of conductive gels or pin-shaped electrodes. Recently, SSVEP detection based on the NHB EEG has been validated and applied in a BCI speller [62]. The online performance of the NHB SSVEP speller could reach 30 bit/min using solely the mastoid areas. Another potential use of NHB EEG is drowsiness detection. In our pilot study, we have demonstrated accessing EEG features associated with neurocognitive drowsiness from the NHB EEG, and those NHB EEG features could achieve the comparable efficacy of discriminating trials with short- vs. long RT in response to lane-departure events to the whole-scalp EEG [63].

This study aims to comprehensively investigate and validate the feasibility of using the NHB EEG as biomarkers for continuous tracking and detection of neurocognitive drowsiness. First, we assessed the drowsiness-related information available in the EEG by a comparison between the EEG correlates of drowsiness from the whole-scalp and those from the NHB channels. Next, we used the drowsiness-related

NHB EEG features to develop a framework for drowsiness detection, and compare the performance of classification using the NHB EEG with that of using the whole-scalp EEG. Finally, we validated the performance of the proposed NHB montage for drowsiness detection with cross-session validation on 10 subjects performing lane-keeping driving experiments.

3.2 Materials and Methods

3.2.1 Behavioral Data Labeling

In the lane-departure event, the level of drowsiness in that given moment was quantitatively estimated based on the RT, which defined as the time between the deviation onset and the wheel-steering onset. For each subject, the RT in each lane-departure event was named local RT, which represents the short-term level of drowsiness. On the other hand, the long-term level of drowsiness was defined by global RT, which was calculated by averaging the RTs across all trials within a 90-second window before the onset of the deviation [19]. For each driving session, the ‘alert RT’ was measured as the 5th percentile of local RTs across the entire session, representing the RT that the subject could perform during alertness. Trials with both local and global RT shorter than 1.5 times alert RT were categorized as ‘alert’ trials, whereas those with both local and global RT longer than 2.5 times alert RT were labeled as ‘drowsy’ trials. The total numbers of alert and drowsy trials were 2,940 and 1,512, respectively, across 10 subjects.

3.2.2 EEG Processing

Six electrodes, Fp1, Fp2, F7, F8, A1, and A2 were placed on NHB areas (see Figure 3.1). All EEG data were re-referenced to the arithmetic average of Fp1 and Fp2.

F7, F8, A1, and A2 were noted as the NHB channels for further analysis. To be specific, F7 and F8 measured the brain activity in the frontal area, while A1 and A2 recorded the brain activity in the left and right mastoid areas, respectively. The EEG signal of each channel underwent a 1-50 Hz band-pass finite impulse response filter to remove low-frequency DC drifts and power line noise at 60 Hz. The filtered EEG data were then down-sampled to 250 Hz to reduce computational load. The data were then cleaned by the procedure of artifact subspace reconstruction (ASR) [44] provided in EEGLAB [45]. The ASR detects high-variance signal components above a given threshold and linearly reconstructed by the retained uncontaminated signal subspace based on principal component analysis (PCA) of 1-min calibration data [64].

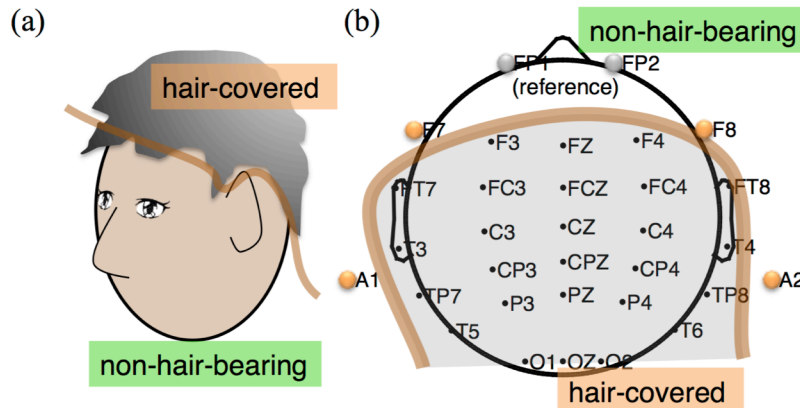


Figure 3.1: (a) The partition of hair-covered areas and non-hair-bearing area divided by a brown boundary. (b) The layout of electrode locations of the 32-channel recording system. Brown boundary separates the divisions of hair-covered and non-hair-bearing area.

3.2.3 EEG Feature Extraction

The EEG features related to neurocognitive drowsiness have been investigated in numbers of previous studies [16][17][18][19][37][51][65], and have been extended into

BCI applications for predicting the human performance in a sustained attention task [17][19][37][65]. As suggested in the preliminary study [63], we employed the EEG data prior to the onset of the task event as features for building a predictive model that can continuously estimates the performance index without relying on any EEG activities induced by infrequent and unexpected events. In this study, theta (4-8 Hz), alpha (8-13 Hz), and beta (13-30 Hz) logarithmic powers of 3s-long pre-event EEG before each lane-departure event were exploited for classifying the ‘alert’ vs. ‘drowsy’ on the upcoming lane-departure event [63]. For each trial, the logarithmic powers of the 3-s pre-lane-departure sub-band-passed EEG segments were estimated. Then, the sub-band logarithmic powers were smoothed to eliminate unrelated spectral perturbations. Finally, both the unsmoothed and smoothed pre-event logarithmic theta, alpha and beta powers for all-channel (AC)/NHB channels congregated a 180/24-dimensional feature set for drowsiness detection. Essentially, the AC montage represents the conventional whole-scalp BCI setting that includes EEG data acquired from both the hair-covered and the NHB areas. A series of analyses and classification experiments was performed in order to quantitatively assess and compare the validity of drowsiness detection based on the AC and the NHB montages.

3.2.4 EEG Classification

Three classic classification methods, linear discriminant analysis (LDA), k nearest neighbors (kNN) and support vector machine (SVM) that have been widely used in EEG classification were employed in this study to discriminate the EEG activity of drowsy state from that of alert state.

(A) Linear Discriminant Analysis

LDA aims to project data onto hyperplanes for maximizing the separation between data from different classes while minimizing the variance of data within the same class [66]. According to statistics, LDA is the most commonly used classification method in BCI studies [67]. Because of its low computational requirement and efficiency, LDA is an ideal simple tool to perform classification for online BCI systems. Nonetheless, the simplicity of LDA is also its drawback as it could fail in dealing with non-linear EEG data [68]. We applied the conventional LDA combined with maximal likelihood (ML) classification that has been used in the preliminary study [63].

(B) k Nearest Neighbors

The kNN classifier is a non-parametric instance-based approach for classifying a sample in the feature space [69]. In the kNN classification, the class of a sample is determined by a majority vote of its k neighboring samples. However, kNN algorithms are known for their sensitivity to curse-of-dimensionality, and are not as widely used in BCI researches as LDA or SVM [70]. We included kNN in this study for the sake of diversity of classic classifiers, where k=5 has been pre-optimized empirically.

(C) Support Vector Machine

SVM is the second most used classifier in BCI studies [67]. Analogous to LDA, SVM also maps data upon a hyperplane, whereas it selects the hyperplane that maximizes the margin between different classes [71]. One advantage of SVM is the generalizability resulted from margin maximization that prevents over-fitting and curse of dimensionality [68], which is crucial for classifying EEG data. The flexibility of kernel selection allows

SVM to handle complex data, but optimizing the parameters could be a time-consuming task. In this study, we used LIBSVM [70] with a linear kernel and grid-search optimization on 5-fold cross validation. The SVM classifier has been used in previous BCI applications for real-time EEG classification [72][73][74].

3.4 Results

Figure 3.2 shows the topographical distribution of Pearson correlation coefficients between the DI and the pre-event EEG power at different frequency bands. In particular, strong EEG correlates of RTs could be found in the frontal theta (negative correlation) and parietal-occipital alpha (positive correlation). The broad distribution of strong EEG correlates (red and blue on the scalp topography) suggests that the informative drowsiness-related EEG dynamics could be extracted from both the hair-covered and the NHB areas.

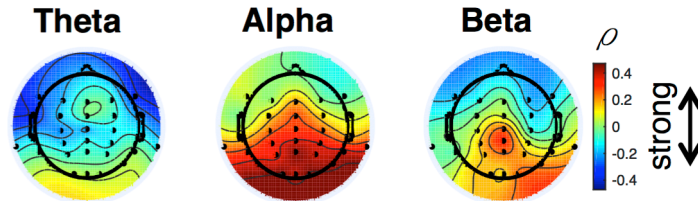


Figure. 3.2: The scalp topography of correlation distributions that exhibits the correlation coefficients (ρ) between normalized RT and pre-event EEG power features of theta, alpha, and beta band at different channel locations across subjects. Strong drowsiness-correlated EEG dynamics, particularly at frontal theta and parietal-occipital alpha, disperse across whole scalp, including both hair-cover and NHB areas.

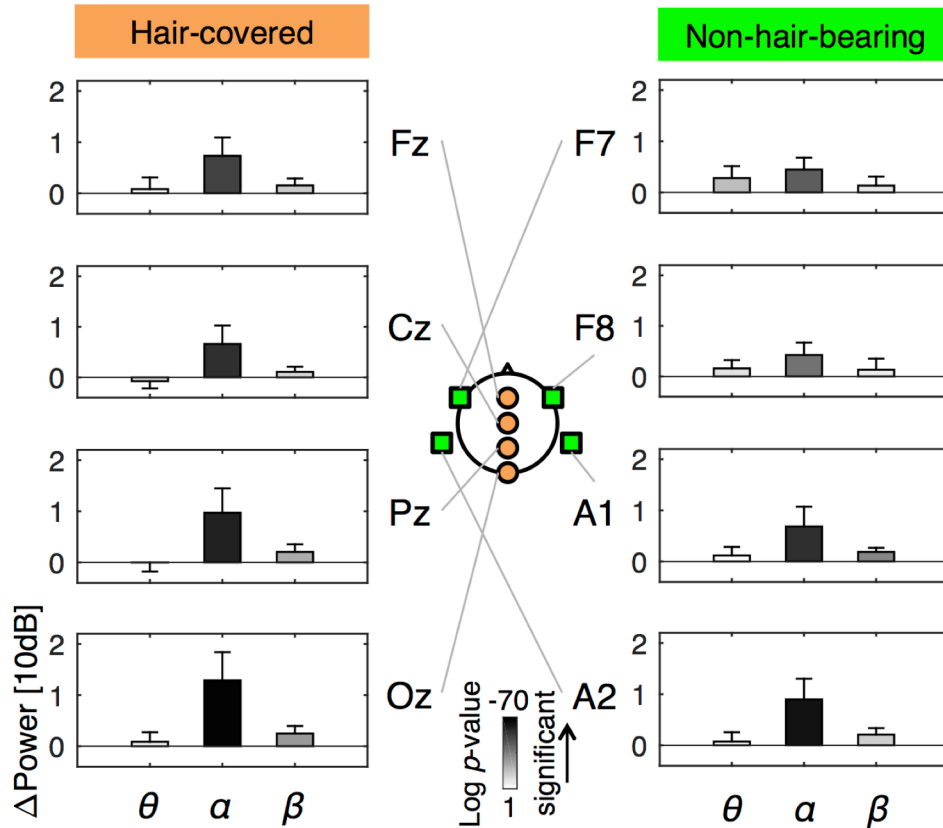


Figure. 3.3: EEG spectral changes from alertness to drowsiness at different representative channels and frequency bands. Bar plots illustrate the average increments across subjects of band power from the alert state to the drowsy state, and error bars mark standard deviations. The spectral increment for each band is calculated by averaging the logarithmic band powers of the 3-s pre-lane-departure EEG across all trials from the drowsy state, and subtracted by the mean logarithmic band power of alert trials. The gray scale filled in each bar indicates the p -value of two-sample t -test for the significance of the difference between the average log-powers of alert and drowsy states. In the left column, Fz, Cz, Pz, and Oz are four representative channels selected from the hair-covered areas, while in the right column, F7, F8, A1, and A2 are four NHB channels utilized for drowsiness detection. Although the increments of powers are more evident at the hair-covered channels than those at the NHB channels, both hair-covered and NHB channels exhibited highly significant power increases in the alpha band.

To validate the significance of drowsiness-related EEG features in the NHB areas, the spectral changes of pre-event EEG between short-RT and long-RT trials at the NHB channels were compared with those at the selected hair-covered channels in Figure 3.3. The statistical analysis indicates strong discriminative features, in particular at the alpha band in both the hair-covered and NHB areas. Table 3.1 summarizes the spectral

differences in pre-event EEG between alert and drowsy state. Though the spectral differences of the NHB EEG between short- and long-RT trials were slightly weaker than those of hair-covered EEG (at Oz), the NHB EEG features are comparable to hair-cover EEG features in the statistical strength of discriminating drowsy state from alert state, which supports the feasibility of using NHB EEG to detect drowsiness.

Figure 3.4 shows the performance of drowsiness detection for a sample session (second session of subject 9, S9-2). Figure 3.4(a) illustrates the fluctuations of global RTs during the entire driving session, where red crosses mark drowsy trials. The driving performance of S9 in the session gradually declined and entered a drowsy state ~70 minutes on the task. Figure 3.4(b) exhibits the prediction of alert/drowsy trials of this session. In the first half of the session, NHB-SVM and AC-SVM have successfully classified the EEG spectra without any false alarm, whereas LDA and kNN classifiers both made some erroneous classifications. From ~70 minute onwards, all approaches detected drowsiness at the transition point of the subject's neurocognitive state. In the later part of the session, as the subject's state shifted back and forth between drowsiness and alertness, all these classifiers predicted drowsy trials correctly, and erroneous predictions tend to occur during the transitions between states. The ROC curves of drowsiness detection of the sample session (S9-2) using the LDA and the SVM were compared in Figure 3.5.

Table 3.1 Power Difference of EEG Features between Alert and Drowsy State

		Δ Power (dB)		
	Channel	Theta	Alpha	Beta
Hair-covered	Fz	0.82±2.30	7.33±3.61	1.54±1.37
	Cz	-0.74±1.45	6.60±3.67	1.08±1.03
	Pz	-0.01±1.78	9.71±4.82	2.05±1.51
	Oz	0.87±1.88	12.88±5.56	2.50±1.48
NHB	F7	2.79±2.36	4.47±1.77	1.33±1.77
	F8	1.59±1.66	4.24±2.21	1.33±2.21
	A1	1.19±1.68	6.87±3.88	1.87±0.82
	A2	0.73±3.88	8.98±4.07	2.10±1.29

Bold: $p < 0.001$, two-sample t test.

Table 3.2 Overall Accuracy of Drowsiness Detection using Within-Subject Cross-Session Validation

Montage	Accuracy (%)		
	SVM	LDA	k NN
NHB	80.0±8.6	79.4±8.7	77.3±10.7
AC	83.3±7.4	78.1±11.9	75.3±12.6

Table 3.3 Overall AUC of Drowsiness Detection using Within-Subject Cross-Session Validation

Montage	AUC	
	SVM	LDA
NHB	0.8576±0.0753	0.7312±0.1412
AC	0.8759±0.0757	0.7758±0.1041

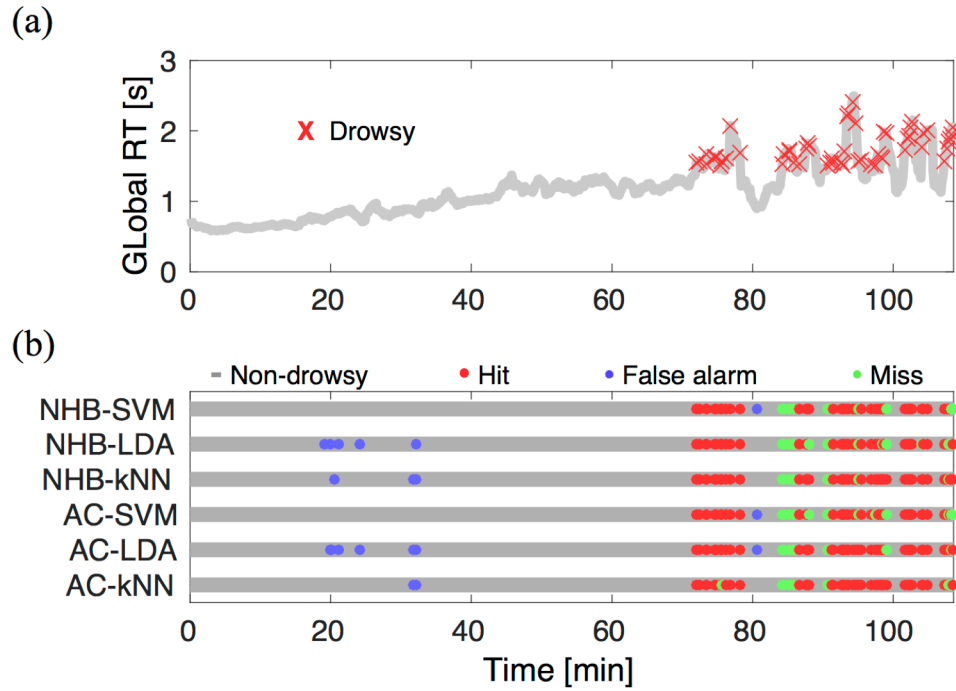


Figure. 3.4: (a) The change of global RT across an entire session of subject 9. Gray line shows the interpolated global RT using the global RT of neighboring trials. Red cross indicates the events that are labeled as ‘drowsy’. (b) The classification results of drowsiness detection using three types of classifier (SVM, LDA, and k NN) with NHB and AC EEG for the same session as in (a). Hit, false alarm, and miss were marked as red, blue, and green dots, respectively. Note that drowsiness detection was performed only at the time right before a lane-departure event presents. The non-drowsy outcome was denoted as a gray belt, which includes the ‘alert’ predictions and other non-drowsy intervals, such as cruise driving and wheel-steering.

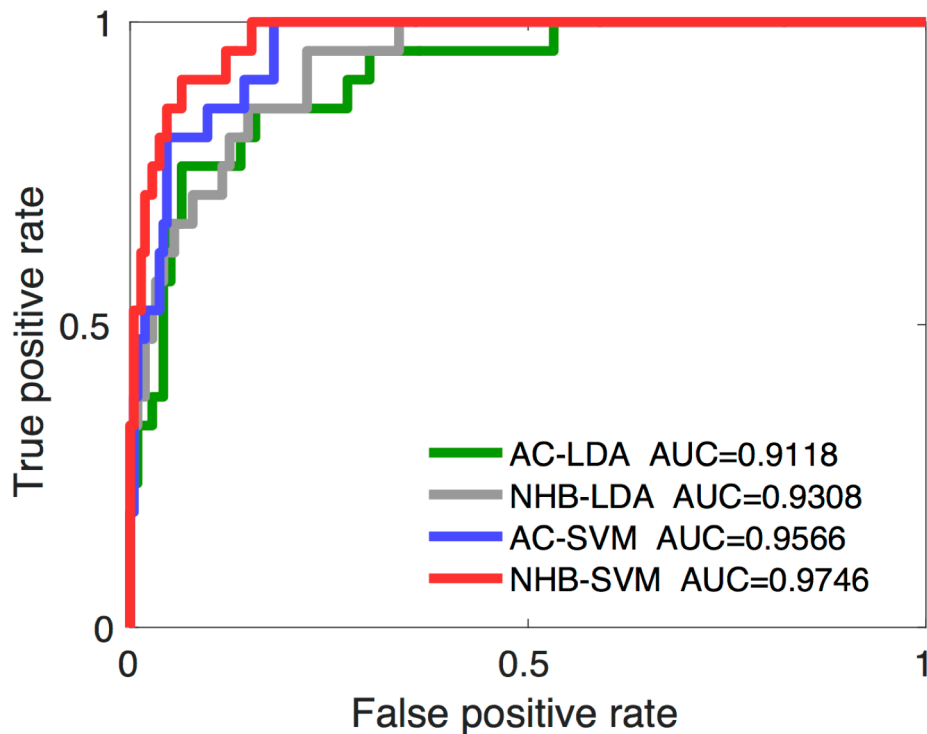


Figure. 3.5: ROC curves describing the relation between true positive rate (sensitivity) and false positive rate (specificity) using NHB EEG and AC EEG with different classifiers on subject 9. Note that positive refers to drowsiness.

Finally, the performances of alert/drowsy classification obtained by three types of classifier using the NHB EEG and the AC EEG were tested by within-subject cross-session validation. Figure 3.6 and Table 3.2 compare the averaged accuracies across all subjects using different montages combined with different classifiers. Two-way ANOVA was applied for analyzing 1) the difference among classifiers and 2) the difference between using the NHB and the AC EEG. The test results show no significant difference in the accuracy between using the NHB and the AC EEG, nor among the three classifiers (Two-way ANOVA, $p=(0.31, 0.16)$). Furthermore, the area under the ROC curve (AUC) is jointly employed to evaluate the classification performance and summarized as in

Table 3.3. Tested by two-way ANOVA, the overall AUC across subjects presents significant difference between the classifiers ($p<0.01$) but no significant difference across between the NHB and AC montages ($p=0.34$).

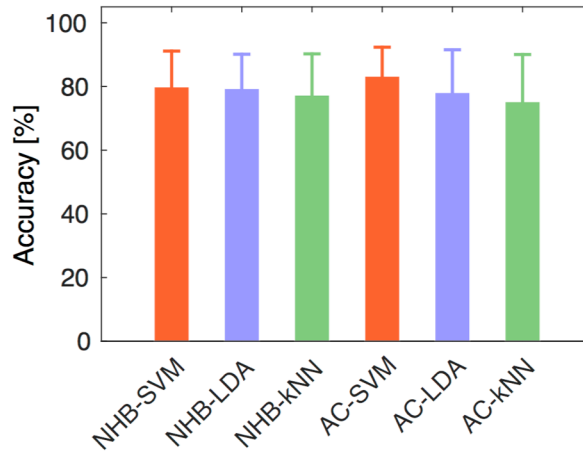


Figure. 3.6: The bar plot compares the average accuracy of drowsiness detection with standard deviation using different metrics across subjects. No significant difference was found between the NHB and the AC montages, nor among the three classifiers (Two-way ANOVA, $p=(0.31, 0.16)$).

3.5 Discussion

In this study, we proposed using a novel EEG recording montage in NHB areas for future BCI applications featuring convenience, economy, and long-term sustainability. Although the concept of drowsiness-related EEG features in the NHB areas has been proposed in our preliminary study on a small group of subjects, the efficacy of using the NHB EEG for BCI applications remains unclear. We hereby comprehensively validated the performance of drowsiness detection based on the NHB EEG across sessions (days).

Furthermore, several widely studied BCI classifiers were employed and compared quantitatively in their performances of drowsiness detection between using the NHB and the whole-scalp montage. Study results suggested that the NHB EEG could provide comparable performance in drowsiness detection to that of the AC EEG regardless of the classifier being used.

It has been shown that drowsiness-related EEG activities could be assessed from various areas over the scalp [17][18][19][75]. For instances, EEG correlates of drowsiness have been identified and validated in frontal theta [75] and parietal-occipital alpha [17][18][19]. The experimental results of this study confirmed the topographical distribution of drowsiness-related EEG features (Figure 3.2), which plays a key role in facilitating the design and use of the NHB EEG-based drowsiness detection. According to the study results shown in Figure 3.3 and Table 3.1, both the NHB and the AC EEG exhibited highly significant spectral differences between alertness and drowsiness. To make a fair comparison on the efficacy of the EEG-based drowsiness detection, we used the same types of electrodes to acquire the AC and NHB EEG simultaneously. This study provides an objective evidence of the feasibility of current and future implications of the NHB EEG.

Although drowsiness-related features of the NHB EEG showed slightly weaker significances in the spectral differences between alertness and drowsiness compared with those of the hair-cover areas (Figure 3.3 and Table 3.1), the classification accuracy of drowsiness detection obtained from the NHB EEG is still comparable to that obtained from the AC EEG (Figure 3.6, Table 3.2, and Table 3.3). This could be explained by the

intrinsically low spatial specificity of EEG recording, which leads to high signal similarity among different channels [76]. As mentioned above, drowsiness-related brain activity is widely spread across a large scalp area, and thus could be assessable from either the hair-covered areas or the NHB areas. The promising findings could encourage further explorations of BCIs based on the NHB EEG. For instance, based on these experimental results, one could develop an NHB BCI that continuously monitors a driver's cognitive state, and mitigates the driver's drowsiness by delivering arousing feedback or other stimulations during the transitioning from alertness to drowsiness [39][77]. This study exploited only the pre-event EEG spectra to discriminate alertness vs. drowsiness of the participants, because drowsiness is most likely to occur during monotonous, uneventful driving in real life. It is impractical to use and rely on EEG spectra following lane-departure events, as they might not present frequently in real driving. Therefore the data processing and analysis for validating the performance of drowsiness detection in this study was designed within a real-world scenario with online applicability. Meanwhile, it is intriguing to investigate how early the drowsiness can be detected in the future work. This could be examined by inserting a varying gap between the data being used for classification and the lane-departure event. As the first attempt made for monitoring human cognitive state related to driving performance using the NHB BCI, the extensions of this study could emerge for other tasks that require maintenance of continuous attention [78].

As the recording area is smaller than using the whole scalp, the wearable device for NHB BCIs is expected to be lighter, more portable, and easier to wear. In addition, the cost of small number of electrodes required for an NHB BCI could be lower than that

of a high-density montage. In fact, consumer wearable devices that acquire EEG signals from NHB areas, such as Neurosky XWave [79] and InteraXon Muse [80], have been commercially available, and their prices are considerably lower than that of the commercial products featuring whole-scalp recording such as [81]. Another advantage of using NHB EEG is that the NHB areas are favorable for most dry or semi-dry EEG electrodes since it has low impedance of skin-electrode contact. For instances, dry Ag/AgCl electrodes, disposable paste ECG electrodes, or patch sensors all prefer or require hairless surfaces. In particular, the recent advance of epidermal sensor patches has made long-term biometric measurements possible in the real world with their softness and deformability [25][26]. The epidermal sensor patches could facilitate maximal comfort in long-term signal acquisition, but are not applicable in the hair-covered areas.

Still, there is a limitation of building a BCI based on the NHB EEG, since most of the EEG activities that have been studied were assessed from hair-covered areas. For certain brain responses that are locally distributed in the central area, the NHB EEG might have low signal-to-noise ratio. Furthermore, as the spatial distributions of brain activities vary across individuals [35][36], the NHB BCI might face severe challenges in maintaining robustness across individuals. The efficacy of NHB EEG requires further investigations on different types of brain activities. In view of these considerable advantages of using the NHB EEG in real-world applications, there is a need for further explorations on what information are available from the NHB areas and what applications could be facilitated using the NHB EEG.

3.5 Conclusion

The current study presented the efficacy of using EEG features that are easily accessible from the NHB areas of the scalp for assessing driving drowsiness. To explore the amount of drowsiness-related information available in the NHB EEG, we quantitatively showed that the spectral differences between alertness and drowsiness in the pre-event (lane-deviation) EEG obtained from the NHB areas are slightly weaker than that obtained from the AC areas. Nonetheless, the drowsiness-related information from the NHB EEG was sufficient to provide comparable drowsiness detection accuracy to that of using the information from the whole-scalp EEG. In general, replacing the whole-scalp recording with the NHB montage is an important and practical step toward real-world BCIs, as there are considerable advantages on the efficiency of sensors, the flexibility of mechanical design, and the improvement of user experience. We believe this study will ignite many new real-world BCI applications that can benefit from the convenience and informativeness of the NHB EEG.

Acknowledgments

This chapter contains material from “Toward Drowsiness Detection Using Non-Hair-Bearing EEG-Based Brain-Computer Interfaces” by Chun-Shu Wei, Yu-Te Wang, Chin-Teng Lin, and Tzyy-Ping Jung, which has been submitted to *IEEE Transactions on Neural System and Rehabilitation* and is currently under review. The dissertation author was the first investigator and author of this paper.

CHAPTER 4

A SUBJECT-TRANSFER FRAMEWORK FOR PLUG-AND-PLAY DROWSINESS DETECTION

Inter- and intra-subject variabilities pose a major challenge to decoding human brain activity in BCIs based on non-invasive EEG. Conventionally, a time-consuming and laborious training procedure is performed on each new user to collect sufficient individualized data, hindering the applications of BCIs in real-world settings. A subject-transfer framework is thus developed for detecting drowsy state based on a large-scale model pool from other subjects and a small amount of alert baseline calibration data from a new user. The model pool ensures the availability of positive model transferring, whereas the alert baseline data serve as a selector of decoding models in the pool. Compared with the conventional within-subject approach, the proposed framework remarkably reduced the required calibration time for a new user by 90% (18.00 min to 1.72 ± 0.36 min) without compromising performance ($p = 0.0910$) when sufficient existing data are available. These findings suggest a practical pathway toward plug-and-play brain decoding for drowsiness detection and can enable numerous real-world BCI applications.

4.1 BACKGROUND

A major challenge in decoding human brain activity is the pervasive and elusive human variability, both across different individuals and within the same individual over time [28][29]. Variability among different individuals, or inter-subject variability, reflects individual differences in brain anatomy and functionality, as each individual has a unique brain [27]. In fact, even monozygotic twins who are genetically identical ultimately have different brain developments due to the influence of varying environmental factors [47].

Because of inter-subject variability, conventional approaches to decoding brain activity in BCIs based on EEG generally require a training phase with pilot data from a BCI user before each execution [1][3][8]. The amount of required training data depends on the type of task and the number of task conditions, and it is often time-consuming and labor-intensive to collect sufficient amounts of data for building a model that recognizes specific brain activities. The tediousness resulting from the training phases amplifies inconvenience of use and unsatisfactory user experience, hindering the practicality of BCI applications in the real world [28]. Some common observable brain patterns across individuals, such as steady-state visual evoked potential and P300, support training-free BCIs [82][83][84] that achieve fairly acceptable performances, but individualized data are still required to further improve the information transfer rate [8][85]. Furthermore, individualized training data might not consistently support robust brain decoding because of intra-subject session-to-session variability, although the intra-subject variability is considered to be less than inter-subject variability [86]. The time-consuming and

indispensable training procedure of conventional BCIs, which often cannot guarantee satisfactory performance, has become the Achilles’ heel of real-world BCI applications.

Recently, efforts have been made to reduce brain-activity decoding schemes’ dependence on individualized training data. Table 4.1 lists several representative studies that focused on reducing calibration time for BCIs. Depending on whether the individualized data from a new user is required for the BCIs, the schemes for reducing calibration time can be categorized into subject-independent (no individualized training data are required from a new user) and subject-dependent (individualized data are required from a new user) methods, as summarized in Table 4.1.

Table 4.1 Representative studies dedicated to calibration time reduction for brain decoding

Study	Task	Subject-dependent	Task-based calibration
Fazli et al., 2009 [30]	Motor imagery		
Lotte and Guan, 2009 [87]	P300 speller	⊙	⊙
Lu et al., 2009 [88]	P300 speller		
Reuderink et al., 2011 [31]	Motor imagery		
Devlaminck et al., 2011 [89]	Motor imagery	⊙	⊙
Tu and Sun, 2012 [32]	Motor imagery	⊙	
Wu et al., 2013 [90]	Stroop task difficulty	⊙	⊙
Samek et al., 2014 [33]	Motor imagery		
Kang and Choi, 2014 [91]	Motor imagery	⊙	⊙
Dalhoumi et al., 2014 [92]	Motor imagery	⊙	⊙
Arvaneh et al., 2014 [93]	Motor imagery	⊙	⊙
Lotte, 2015 [34]	Motor imagery	⊙	⊙
Morioka et al., 2015 [28]	Visual-spatial attention	⊙	

A subject-independent BCI could be achieved by a robust feature-extraction method that reduces the inter-subject variability in the features used for decoding brain

responses [30][31][32][33]. Subject-independent approaches allow BCIs to operate without any calibration data from a new user, and thus enable so-called “plug-and-play” BCIs [94]. However, loss in performance is inevitable in those subject-independent approaches, compared to the individualized training-session approaches [30][31]. On the other hand, the subject-dependent approaches utilize a small amount of individualized training data to reduce subject-to-subject variations and loss in performance, in contrast with the individualized training-session approaches that require an entire training session. The calibration data can be reduced by using only a few trials from each class in the BCI task [34][89][91][92][93], or by using only a subset of classes with a regularized feature-extraction method that improves the robustness of the covariance matrix estimation for model training [87]. However, with such a small amount of training data, it is relatively difficult to extract signals of interest from arbitrary noise, raising a challenge of maintaining decoding performance. To improve the performance of subject-dependent approaches with minimal individualized calibration data, one strategy is to expand the size of existing data from other (source) subjects, and then to leverage the large-scale data using subject-transfer techniques for a new (target) subject [34]. The subject-to-subject transfer of BCI models can be regarded as a scheme of transfer learning as it reuses the existing knowledge to deal with a new domain [95].

The materials transferrable across subjects could be the neurophysiological measurements, the filters, and/or the classifiers [29]. Because the inter-subject variability might lead to deterioration in the efficiency of transferring decoding models across subjects, it is necessary to selectively utilize data within the existing dataset. A previous work suggested finding auxiliary data from other subjects that are similar to the target

subject's data to train a robust decoding model [90]. Later on, ensemble approaches were proposed to combine the classification models from source subjects into a new model for the target subject [34][92][93]. Yet, the subject-transfer approaches mentioned above require a supervised task-based training session to collect the task-relevant individualized calibration data. In real-world applications, it is inconvenient to perform task-based training sessions repeatedly. Moreover, the task-relevant data might not even be available in some cases of brain state monitoring. For instance, there have been laboratory-based BCIs developed for alertness/drowsiness monitoring that requires data recorded in both alert and drowsy states [17][19][50][96], but asking an awake subject to enter the drowsy state successfully in a short time is essentially impractical. Therefore, it might not be realistic to include all state-related data from the target subject to expedite the calibration of a brain-state monitoring BCI with real-world settings.

While task-based calibration is often time-consuming and expensive, task-free brain activity observed while the subjects are not engaged in any specific task has been shown to exhibit patterns of functional connectivity [35][36]. In a cognitive experiment, task-free brain recording is available during resting or passive stimulation conditions (e.g., naturalistic viewing) [97]. Several studies have explored the extent to which task-free activity can be used to improve the performance and the practicality of BCIs [28][98][99][100][101][102]. For instance, the independent components extracted from resting-state EEG can provide motor-related spatial filters for a motor-imagery BCI with high accuracy comparable to those obtained by using task-relevant calibration data [99]. Also, the resting-state measurements have been applied to predicting individual differences in BCI performances [98][99][100][101][102]. Lately, resting-state EEG was

involved in a subject-transfer framework proposed for reducing the calibration efforts of spatial attention decoding [28]. Inspired by these studies, we assumed that information about state-related brain dynamics could be inferred from baseline EEG traits. Thus, the subject similarity in EEG power spectra under an alert baseline condition could be useful to estimate subject similarity in drowsiness-related brain response. In that case, as the alert baseline can be easily collected, it enables a near-zero-calibration BCI by leveraging baseline similarity and decoding models from other subjects.

In this study, with a focus on drowsiness detection, we propose leveraging data from other subjects to tackle intra-subject variability in building brain-state decoding models, and utilizing a small amount of baseline data from a new user to deal with inter-subject variability in drowsiness-related brain response. The working hypothesis is that similarity in state-related brain dynamics among individuals is predictable by alert baseline EEG. If the hypothesis holds, such predictability can be used to ensure positive transferring of brain-state decoding models among subjects, thus improving the efficiency of the subject-transfer approach. Furthermore, if large-scale existing data are available, it might be feasible to identify supportive data or models from other source subjects in the dataset using the alert baseline EEG from the target subject. We therefore extended the results from our preliminary study [43], and the major contributions are threefold. First, we proposed using hierarchical cluster analysis to explore the associations between EEG features and cognitive states to assess the inter- and intra-subject variabilities of state-related brain dynamics across subjects and sessions. This will lay the foundation for a subject-transfer framework with a large-scale dataset for individualized brain-state decoding and monitoring. Second, we investigate the effectiveness of alert baseline EEG

activity in predicting the similarity of EEG-state associations among subjects, which plays a key role in minimizing the calibration effort for a new target user. Finally, we proposed and validated a subject-transfer framework that leverages baseline EEG and large-scale existing data to facilitate individualized brain-state decoding with minimal calibration effort.

4.2 Materials and Methods

A subject-transfer framework was proposed to leverage the existing source models (the EEG-DI models of source sessions) in the pool to reconstruct a new decoding model for a new target subject, as shown in Figure 4.1. The proposed framework is based on two fundamental assumptions:

A1) When sufficient existing data from other subjects are available, it is possible to obtain high decoding performance (i.e., the predictive performance of an EEG-DI model) by transferring one or multiple source models to the target session. The decoding performance obtained using the subject-transfer approach might be comparable to that using a self-decoding model that is trained by the drowsiness-related data from a pilot session of the same subject.

A2) The alert baseline EEG activity provides useful information for predicting inter-subject similarity in state-related brain responses. If so, one can select supportive sources models based on easily collected baseline data from the target subject.

According to A1, a large-scale source model pool is required to maximize the chance to identify supportive source models from the pool. Otherwise, the subject-transfer approach might be unable to compete with the conventional self-decoding approach. Regarding the validity of A2, the alert baseline EEG activity can be easily

acquired when a subject is not engaged in any task. In the LKT driving experiment, the alert baseline is available during cruising before a lane-departure event occurs.

For each session in the selected dataset of 54 sessions from 25 subjects, an EEG-DI decoding model was constructed with EEG band powers and DI labels as described above. Meanwhile, the alert baseline was obtained from the inter-trial cruise-driving period of the first 10 trials at the beginning of the driving session. As each trial provides a 120-dimensional vector of band power features, we took the median across the first 10 trials, and then linearly scaled into a 1×120 vector of power distribution density, F , with a sum equal to 1.

4.2.1 EEG-DI Regression Models

For each LKT session, a decoding model was trained to predict the DI for each upcoming lane-departure event based on the above-mentioned associations between the DI and EEG spectral features. To eliminate the high co-linearity and dimensional redundancy of multi-channel EEG data, PCA) was involved prior to the regression models, as PCA has been shown able to reduce noise and computational load with an adequate selection of principal components [17][103]. Furthermore, applying PCA could also alleviate curse-of-dimensionality in building such predictive models [68]. In this study, we retained the principal components that account for 90% of the explained variance in the data [17][43], and then the PCA-reduced features were used as the predictors in the regression model to predict the DI. Two conventional regression approaches, ordinary least squares linear regression (LR) and support vector regression (SVR) with a linear kernel, were applied and compared in this study. The SVR was implemented using LIBSVM [70] with grid-search optimization on leave-one-session-out

cross-validation. Each driving session provides one EEG-DI decoding model, including the PCA and the regression, and is transferrable to other subjects. In this study, the decoding performance of the EEG-DI model is evaluated by the Pearson’s correlation coefficient (ρ) between the actual and predict DI across an entire session.

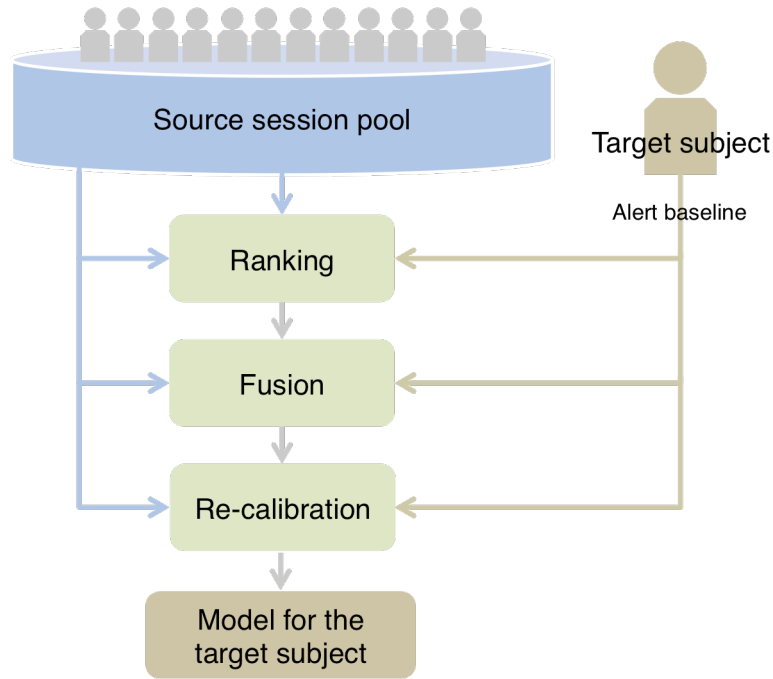


Figure 4.1: An illustration of the proposed subject-transfer framework. A source model pool is constructed based on the existing data collected from the source (other) subjects. This framework also includes the optimization mechanism for ranking and fusing source models for each of the target subjects (see main text).

4.2.2 Multiple Distance Measurements

We utilized classic distance metrics to estimate the (dis)similarity in alert baseline EEG among different subjects [104][105][106][107][108]. In addition to the alert baseline activities, as the EEG-DI models are prepared for each session in the pool, we also calculated model ‘transferability’ for each source model, which refers to the overall predictive performance of the source model on all the sessions from other subjects in the pool [43]. This was done by measuring the distance using the power distribution density,

F , across subjects. We then defined a multiple distance measurement (MDM) that involves the distances of alert baseline EEG and model transferability among subjects. Given a source session indexed by ‘ a ’, and a target session indexed by ‘ b ’, six distance metrics were involved to calculate and construct the MDM between their alert baseline power distribution, F_a and F_b . The expressions of the distance metrics can be found in the following subsections.

1) Euclidean distance

The ordinary Euclidean distance measures the distance between the two vectors as between two points in the space with the formula:

$$D_{Euclidean}(\mathbf{a}, \mathbf{b}) = \sum_i (F_{a_i} - F_{b_i})^2$$

where F_{a_i} denotes the i -th element in the vector F_a

2) Correlation distance

The correlation distance is defined as one minus the Pearson’s correlation coefficient between two vectors. Pearson’s correlation has been commonly used to measure the similarity of EEG spectral distributions [43][104].

$$D_{correlation}(\mathbf{a}, \mathbf{b}) = 1 - \frac{\sum_i (F_{a_i} - \overline{F_a})(F_{b_i} - \overline{F_b})}{\sqrt{\sum_i (F_{a_i} - \overline{F_a})^2} \sqrt{\sum_i (F_{b_i} - \overline{F_b})^2}}$$

3) Chebyshev distance

Chebyshev distance measures the maximal elemental distance between two vectors by:

$$D_{Chebychev}(\mathbf{a}, \mathbf{b}) = \max_i (|F_{a_i} - F_{b_i}|)$$

4) Cosine distance

Cosine distance is expressed by one minus the cosine similarity between two vectors.

$$D_{\text{cosine}}(\mathbf{a}, \mathbf{b}) = 1 - \frac{\sum_i (\mathbf{F}_{a_i} \cdot \mathbf{F}_{b_i})}{\sqrt{\sum_i \mathbf{F}_{a_i}^2} \sqrt{\sum_i \mathbf{F}_{b_i}^2}}$$

5) Kullback–Leibler divergence

Kullback-Leibler (KL) divergence measures the non-symmetric difference between two probability distributions. A previous study has applied the average of bi-directional KL divergence on EEG power distributions to classify EEG under different mental states [106]. Hereby the distance measurement based on KL divergence was estimated using the following equation:

$$D_{KL}(\mathbf{a}, \mathbf{b}) = \sum_i \frac{KL(\mathbf{F}_{a_i}, \mathbf{F}_{b_i}) + KL(\mathbf{F}_{b_i}, \mathbf{F}_{a_i})}{2}$$

where $KL(\mathbf{p}, \mathbf{q}) = \sum_i p_i \log(p_i/q_i)$

6) Transferability-based distance

One measurement of the similarity between a source subject and a target subject could be estimated by overall transferability of a source model calculated by its overall decoding performance on other source subjects [43]. Note that the transferability-based distance is dependent solely on the source model pool. Given a source model pool, the estimated performance-based distance of the source session, \mathbf{a} , is defined as:

$$D_{\text{transferability}}(\mathbf{a}) = 1 - \text{median}(XP(\mathbf{a}, J(\mathbf{a}, \mathbf{M}_{\text{source}})))$$

$$\mathbf{a} \subset \mathbf{M}_{\text{source}}$$

where $J(\mathbf{a}, \mathbf{M})$ denotes the function that outputs the set of all session indices from other subjects of the session \mathbf{a} in the session set, \mathbf{M} , given $\mathbf{a} \subset \mathbf{M}$. $\mathbf{M}_{\text{source}}$ denotes the set of

indices of sessions form the source model pool. $XP(\mathbf{a}, J)$ outputs a vector of cross-subject performances of the model of session, \mathbf{a} , on all the other subjects' sessions, J .

The above-mentioned distance metrics encompass the MDM across sessions. In practice, the MDM between a target session, i , and the source sessions, \mathbf{M}_{source} , is represented as a 6-dimensional matrix:

$$\mathbf{MDM}(i, \mathbf{M}_{source}) = [D_1(i, \mathbf{M}_{source}), D_2(i, \mathbf{M}_{source}), \dots, D_6(i)]$$

where D_1 , D_2 , ..., and D_6 denote $D_{Euclidean}$, $D_{correlation}$, $D_{Chebyshev}$, D_{cosine} , D_{KL} , and $D_{transferability}$, respectively.

4.2.3 Source Model Ranking

To predict the performances of source models on a target session using the MDM, a linear SVR model trained within the source-model pool was employed to assess the relationship between the MDM and the cross-subject decoding performance, or the transferability of the source models. As the effectiveness of each of the above-mentioned distance measures for discriminating alertness and drowsiness was unknown, an SVR can automatically select an optimal combination of those distance measures. A brief flow of training and test process for the transferability predictive model is illustrated in Figure 4.2. To be specific, given a pool of N source models, with a set of indices denoted by $\{\mathbf{i}_1, \mathbf{i}_2, \dots, \mathbf{i}_N\}$, the corresponding alert baseline MDM of the source session, \mathbf{i}_n , to other source sessions from other subjects is expressed as:

$$\mathbf{MDM}(\mathbf{i}_n, J(\mathbf{i}_n, I_{source})) \quad \forall \mathbf{n} \in \mathbf{1}, \mathbf{2}, \dots, N$$

Meanwhile, the transferability of other source models on session \mathbf{i}_n can be obtained by the cross-subject model performances as a vector:

$$XP(\mathbf{i}_n, J(\mathbf{i}_n, I_{source})) \quad \forall \mathbf{n} \in \mathbf{1}, \mathbf{2}, \dots, N$$

For all source sessions available in the pool, $\{\mathbf{i}_1, \mathbf{i}_2, \dots, \mathbf{i}_N\}$, their data of MDM and XP were collected to train a predictive regression model for predicting XP using MDM. Before concatenating the N MDM matrices, each MDM matrix was normalized into z-scores vector by vector. The N XP vectors were similarly normalized and concatenated. Finally, the concatenated MDM and XP were applied as the predictor and the response, respectively, to train a linear SVR model for transferability prediction. For a new target session \mathbf{i}_{N+1} , we used the trained transferability predictive (SVR) model and the baseline distances $\mathbf{MDM}(\mathbf{i}_{N+1}, J(I_{source}, \mathbf{i}_{N+1}))$ to estimate the transferability of all other source models. Based on the estimated transferability, from high to low, we ranked each of the N source models by $\{\mathbf{m}_1, \mathbf{m}_2, \dots, \mathbf{m}_N\} \in \{1, 2, \dots, N\}$.

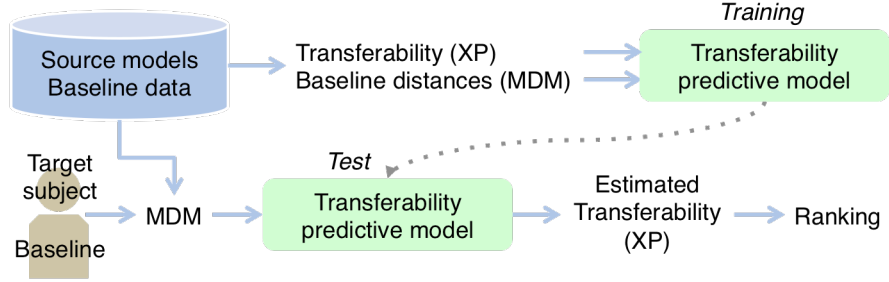


Figure 4.2: The training and test flow of the transferability model for source model ranking.

4.2.4 Model Fusion and Re-Calibration

Given the rankings of the N source models, we proposed a selective weighting scheme to assign large weights to high-ranked models and small weights to low-ranked models. The weights were determined based on a logistic function with tuning parameters for the mid-point and the steepness expressed as follows.

$$W(m, k, l) = 1 - 1/(1 + e^{-k(\frac{m}{N}-l)})$$

where m is the ranking of a source model, $k \in \{10,20, \dots, 100\}$ and $l \in \{0.1,0.2, \dots, 1\}$ are parameters that adjust the steepness and the mid-point, respectively, of the logistic function. The estimation of optimal parameters was obtained using a grid-search mechanism with leave-one-subject-out cross-validation within the source sessions. The fused output of source models was then generated by the following equation:

$$\hat{y} = \sum_{n=1}^N \frac{W(m_n, k, l)}{\sum_{n=1}^N W(m_n, k, l)} \hat{y}_n - \hat{y}_0$$

where \hat{y}_n is the output of the source model n for a given trial, and \hat{y}_0 is an offset estimated by the median of the initial 10 trials (i.e. the alert baseline) in the target session. Here the alert baseline also serves for re-calibrating on the fused model. Note that the brain state in the beginning of a session was supposed to be ‘alert’ according to the criteria of session selection described in Section 2.2.1, Chapter 2.

4.3 Results

As proposed in our framework, alert baseline data were used to identify supportive source models for a target subject. We performed an offline analysis to validate to what extent the similarity in alert baseline activity could predict the transferability of an ensemble of source models to a target subject as shown in Figure 4.3. Using MDM of alert baseline activity between each source session and the target session (S44-4), the transferability predictive model was able to predict the actual transferability score of each source model to the target session. The highly significant correlation ($r^2 = 0.4279$, $p < 10^{-6}$) between actual and predicted performances poses strong evidence that alert baseline brain activity carries information on cross-subject similarity of state-related

brain dynamics. The predictability of source model transferability enables a plausible ranking scheme for the source models based on their alert baseline similarities to the target subject, facilitating positive subject-to-subject transfer in the proposed framework.

Table 4.2 summarizes the decoding performance of DI using different approaches across 17 test (target) subjects in terms of the correlation coefficient (ρ) between actual and predicted DI. Self-decoding (SD) approach refers to conventional within-subject pilot session approach, where the decoding model was trained by the data from a whole pilot session. Subject-transfer (ST) approach utilized models from the source model pool and alert-baseline calibration, which required the alert baseline data from the target subject only. There was no significant difference between SD and ST, neither between LR and SVM ($p = [0.3321, 0.9121]$, 2-way ANOVA), showing that the ST approach achieved comparable performance to that of the SD approach. Figure 4.4 exhibits the decoding results obtained using the ST and self-decoding approaches of a sample session (S54-2). Subject-transfer approach using SVR showed the highest performance ($\rho = 0.7552$) among all decoding approaches. For simplicity, only SVR was involved as the regression method in the following validation of our framework.

Next, we systematically investigated the influence of the source data size on the ST decoding performance across all target subjects. To this end, we randomly reconstructed the source-model pool with a subset of the original source subjects, and redid the subject-transfer procedure with the successively reduced source-model pool. This procedure was repeated 20 times for each reduced size of the randomly reconstructed source-model pool. Figure 4.5 exhibits the relationship between the decoding performance and the number of source subjects in the pool. The overall ST

decoding performance across 17 target subjects (red curve) presents a monotonic increase when the number of the source subjects included in the subset grows, suggesting that large-scale existing data from other subjects could improve the ST decoding performance. The decoding performance of the proposed ST approach reached and exceeded that of the SD approach when the pool size was over 7 subjects, but the difference was not statistically significant ($p > 0.05$). In addition, Figure 4.5 also shows the performance of randomized ST that fused the source models with random weights (gray curve), as opposed to using the ranking scheme based on alert baseline similarity. The ST decoding using the supportive sessions selected by alert baseline similarity significantly outperformed the randomized ST performance ($p < 0.05$, paired t-test) for all the reduced numbers of source subjects in our test.

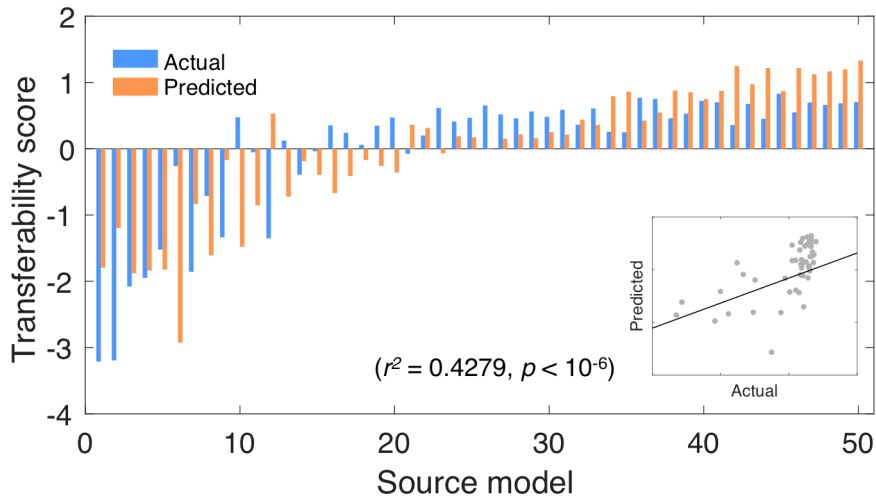


Figure 4.3: Actual (blue bars) and predicted (red bars) transferability scores of source models based on the alert baseline similarity among subjects. The MDM among subjects was able to predict the model transferability evidenced by a highly significant correlation between actual and prediction transferability score ($r^2 = 0.4279, p < 10^{-6}$).

Table 4.2 Overall decoding performance using different approaches

Performance (mean±standard error)	Linear regression	Support vector regression
Self-decoding	0.5808±0.0169	0.5871±0.0719
Subject-transfer	0.6380±0.0095	0.6448±0.0381

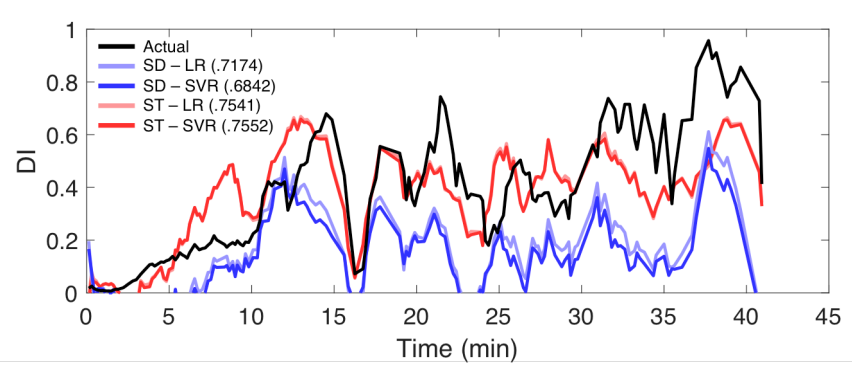


Figure 4.4: EEG-based DI decoding result using self-decoding (SD) and subject-transfer (ST) approaches with LR and SVR of a sample session (S54-2). The calibration time was 89.91 min for the SD approaches and 1.48 min for the ST approaches.

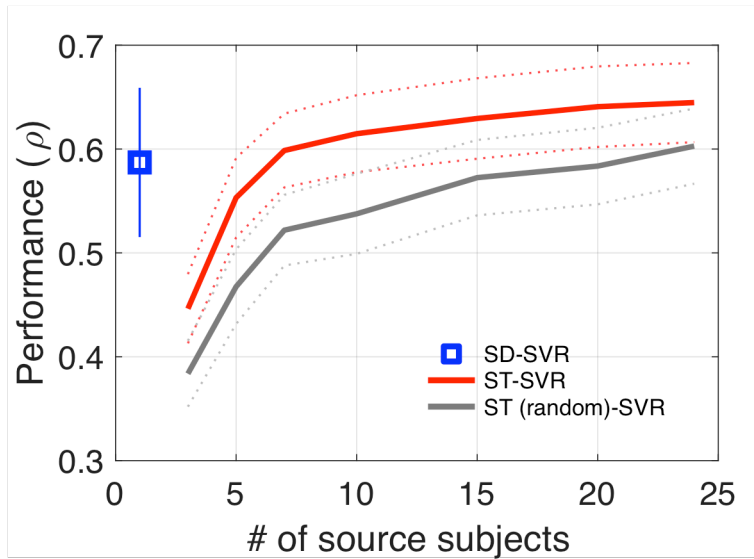


Figure 4.5: The decoding performance of the proposed subject-transfer (ST) approach (the red curve with standard error) as a function of the number of source subjects available in the pool. The gray curve shows the randomized ST performance without source-model ranking. The difference in the overall performance between the ST and randomized ST was significant ($p < 0.05$, paired t -test) across all numbers of source subjects. The proposed ST approach could achieve comparable performance with the SD approach ($p > 0.05$) when the number of source subjects exceeded 7.

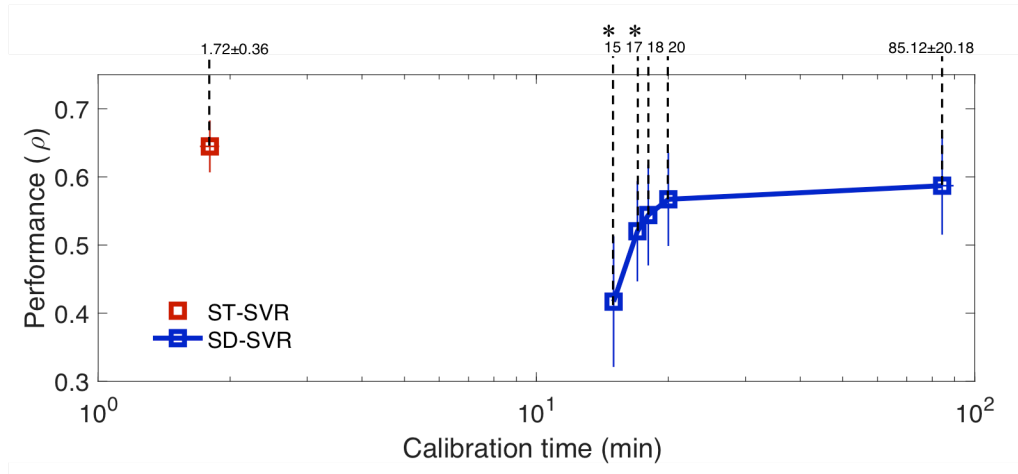


Figure 4.6: A comparison of decoding performance between using the proposed subject-transfer (ST) and the conventional self-decoding (SD) approach in terms of decoding performance (correlation coefficient, ρ), and calibration time across 17 target subjects who performed multiple LKT sessions. Red/blue squares show the overall performance against the calibration time for the ST/SD approach with SVR. When the calibration time of SD approach was less than 18 min, the difference in performance was observed between the ST and SD approaches ($p < 0.05$ by paired t -test). Whereas there was no significant difference in performance between them when the calibration time of SD approach was equal to or larger than 18 min. Thus, the calibration time reduction using the ST approach was estimated by 90% (1.72 ± 0.36 min vs. 18.00 min).

Figure 4.6 shows the decoding performance of the ST approach against the required recording time for calibration data collection, compared to that using different size of individualized drowsiness-related training (pilot) data, as would be the case for the SD approach. The ST approach significantly outperformed the SD approach when the drowsiness-related training time was less than 18 min. This experiment validated the efficiency of the ST approach in calibration time reduction from 18 min to 1.72 ± 0.36 min, the time required for collecting the alert baseline.

4.4 Discussion

This study proposes a subject-transfer framework to minimize the calibration effort for brain-state decoding, particularly for EEG-based drowsiness detection. The experimental results validated the two assumptions underlying the proposed framework. First, the subject-transfer framework that leverages a large dataset from other subjects can achieve comparable performance to self-decoding when the existing data are sufficient. Second, the easily collected alert baseline activity is capable of assessing the similarity of state-related activity from the subjects in the pool, and thus enables a selective fusion of the source models to ensure the efficiency of model transferring.

As shown in Figure 4.3, the predicted model transferability was highly correlated ($r^2 = 0.4279$) with the actual transferability, suggesting that the similarity in EEG-DI associations across subjects is predictable by the similarity in their alert baseline brain activities. Our finding is in accordance with previous studies that suggest the association between brain functionality and task-free activity [35][36][109]. Specifically, task-free data could be used to select supportive task-based models to improve the efficacy of subject-to-subject model transferring for a BCI. Analogously, spectral power in the resting-state EEG was used to predict the individual differences in BCI performances in a previous study [98]. The associations between task-free EEG oscillations and hemodynamics have been investigated using simultaneous EEG/fMRI recording. For instance, resting EEG spectral powers were found associated with the functional networks [110][111], and time-frequency representation of EEG data could be used as a ‘fingerprint’ to predict specific brain activity as measured by fMRI [112]. In line with the

above-mentioned studies, we demonstrate that individualized state-related brain response can be inferred from a rapid alert-baseline calibration, and such relationship enables the applicability of subject-transfer approaches with minimal calibration effort.

As shown in Figure 4.5, we observed that at least 7 source subjects are required to achieve satisfactory performance. The subject-transfer performance monotonically increased as the number of source subjects increased, and reached a slightly better (but not statistically significant) overall performance than that of the conventional self-decoding approach. Previous studies have pointed out the importance of a large-scale dataset (>50 sessions) for subject-transfer approaches [33][34][113], but none of them have quantitatively investigated the influence of the size of existing data on the subject-transfer performance. We have shown that the availability of large-scale data is one of the supportive elements for positive subject-transfer performance. As auxiliary data are more likely obtained from subjects that are similar in EEG-DI associations, the number of source subjects seems to affect the chance to find supportive source subjects for a target subject. The sufficiency of data is also beneficial for the estimation of transferability of the source models, the training of transferability predictive model, and the optimization of fusion parameters in the proposed framework.

The significant reduction in calibration time is the most remarkable perk drawn from the proposed subject-transfer framework for BCI applications. As we introduced the alert-baseline calibration to identify the supportive sessions for model transferring for each target subject for testing, the calibration time for brain-state decoding was reduced by 90%, from 18 min to ~100 s (see Figure 4.6) without compromising decoding accuracy ($p = 0.0910$). It is also worth mentioning that the proposed subject-transfer

framework, which uses alert-baseline calibration to select supportive sessions, is not limited to brain-state-decoding BCIs. Other types of BCI in which task-based calibration is costly and impractical might also benefit from the proposed approach. In fact, during the ~ 100 s of alert baseline activity collection, only 30 s ($3 \text{ s} \times 10$ trials) of data were actually used, indicating the room for further improvement in alert-baseline calibration time. Study results of the current study have demonstrated the efficacy of the subject-transfer framework for detecting drowsiness during a driving task. The framework might also be applicable to other brain-state decoding if the problem domain satisfies the major assumptions (A1 and A2) addressed at the beginning of Section 4.2. However, further work is needed to test to what extent this framework can be generalized to decoding other brain states.

The results of this study suggest the potential of using baseline calibration and large-scale data in brain decoding to deal with inter- and intra-subject variabilities, which is related to the concept of zero-training BCI initialization [113]. As the size of existing data plays an important role in supporting the efficacy of subject-transfer approach, constructing a massive neuroscience dataset seems to be an important prerequisite for translating the findings of this study into real-world applications. Fortunately, effort have been made by researchers in building big databases for neuroscience research [6] [114].

Two decades ago, Jung et al. [17] discussed the issues to be resolved for implementing a practical EEG-based alertness monitoring system. In particular, they pointed out the demand of minimizing the amount of pilot training data from individual subjects. In our proposed framework, we adopted current methods and technologies that tackled those issues and made a significant contribution to the calibration time reduction.

As the methodologies developed in this study are not subject to the purpose of drowsiness detection, further exploration of the generalizability of the proposed subject-transfer framework in other types of brain state decoding is required. With the findings in this study, we expect the subject-transfer framework to ignite further development of plug-and-play brain decoding based on large-scale data and alert-baseline calibration.

4.5 Conclusion

This study presents a subject-transfer framework to minimize the calibration effort in the brain decoding for drowsiness detection while maintaining comparable performance to individualized self-decoding based on a full task-based pilot session. With the subject-to-subject similarity measured by subjects' alert baseline activities and cross-decoding performances, the proposed framework showed high efficiency and efficacy in ranking the existing source models according to their predicted performance on a new user. The experimental results also suggest the importance of data size in supporting positive inter-subject model transferring. As the proposed framework successfully reduced the required calibration time by 90% (18.00 min to 1.72 ± 0.36 min) for drowsiness detection, it can considerably improve the practicality of brain-state-decoding BCIs and lead to many real-world applications.

Acknowledgments

This chapter contains material partly from “Towards Plug-and-Play Brain State Decoding for Drowsiness with Large-Scale Data and Baseline Calibration ” by Chun-Shu Wei, Yuan-Pin Lin, Yu-Te Wang, Chin-Teng Lin, and Tzyy-Ping Jung, which has been

submitted to *NeuroImage* and is currently under review. The dissertation author was the first investigator and author of this paper.

CHAPTER 5

CONCLUSION AND FUTURE WORKS

This thesis summarizes the efforts made for transitioning a DD-BCI to a real-world application with usability and convenience. Specifically, this thesis highlights improvements in the EEG recording montage and the calibration time for initiating the BCI.

A large-scale analysis on the associations between EEG and drowsiness was performed on a multi-subject EEG dataset collected in lane-keeping driving experiments. To gain a thorough understanding of the EEG-drowsiness associations, the correlations between EEG features and a response time-based drowsiness index were visualized using hierarchical cluster analysis. The clustering showed that similar EEG-drowsiness correlations were found among different subjects. This finding suggests the feasibility of transferring decoding models across subjects. Meanwhile, the EEG features appeared similar and redundant across channels in the spatial domain. Therefore, it might be possible to reduce the number of channels for EEG recording without loss in the decoding performance.

For the improvement of brain monitoring montage, the efficacy of NHB EEG in detecting drowsiness was investigated in terms of the EEG-drowsiness correlations. The

drowsiness-related features obtained from NHB EEG were shown capable of supporting satisfactory decoding performance. The validation for the proposed NHB DD-BCI exhibited a comparable accuracy to that using whole-scalp EEG. Reducing from whole-scalp to NHB areas, this novel montage introduces flexibility and convenience for designing the next generation of real-world BCIs.

Human variability in brain activity is a major issue in the development of a plug-and-play BCI with minimal calibration. To obviate inter- and intra-subject variabilities, a subject-transfer framework with large-scale data and baseline calibration was proposed and compared to the conventional self-decoding approach that requires individual task-relevant data. The proposed subject-transfer framework was able to reduce the calibration time by 90% without compromising the performance of drowsiness detection.

Intuitively inferred from the contributions presented in this thesis, one possible future work is to build a plug-and-play NHB DD-BCI with a mini-sized EEG wearable featuring near-zero calibration. This future work would require further validation on the efficiency of the subject-transfer framework with the low-density NHB EEG recording. Another interesting research direction is applying deep learning to drowsiness detection. This new approach might improve the accuracy and robustness beyond the current approach, as deep learning-based EEG classification has recently been shown promising in recognizing motor-imagery patterns [114] and sleep stages [116].

APPENDIX A

SELECTIVE TRANSFER LEARNING FOR EEG-BASED DROWSINESS DETECTION

On the pathway from laboratory settings to real world environment, a major challenge on the development of a robust electroencephalogram (EEG)-based brain-computer interface (BCI) is to collect a significant amount of informative training data from each individual, which is labor intensive and time-consuming and thereby significantly hinders the applications of BCIs in real-world settings. A possible remedy for this problem is to leverage existing data from other subjects. However, substantial inter-subject variability of human EEG data could deteriorate more than improve the BCI performance. This study proposes a new transfer learning (TL)-based method that exploits a subject's pilot data to select auxiliary data from other subjects to enhance the performance of an EEG-based BCI for drowsiness detection. This method is based on our previous findings that the EEG correlates of drowsiness were stable within individuals across sessions and an individual's pilot data could be used as calibration/training data to build a robust drowsiness detector. Empirical results of this study suggested that the feasibility of leveraging existing BCI models built by other subjects' data and a relatively small amount of subject-specific pilot data to develop a BCI that can outperform the BCI based solely on the pilot data of the subject.

A.1 Background

Recent progress in brain-computer interface (BCI) has been made in a great variety of applications [2]. Electroencephalogram (EEG)-based BCIs have begun to seek real-life applications. For example, several BCI studies have proved the feasibility and practicability of detecting an individual's drowsiness level using spontaneous EEG activities [17][21][41]. Nevertheless, promising results of the offline prediction were just a first step on the pathway toward real-world applications.

A major challenge in moving BCIs from well-controlled laboratory settings to real-world environments is that most of the BCIs require a significant amount of training data to build an accurate and robust model for each individual, which is labor-intensive and time-consuming and thereby significantly hinders the applications of BCIs in real-world settings.

Taking EEG-based drowsiness estimation as an example, the pilot data collecting session could be very long and tedious because the pilot session for each individual must contain a representative variety of drowsiness levels. It is thus imperative to develop a method to reduce the amount of training data needed from each individual for drowsiness detection BCI. An obvious alternative is to leverage existing data from other subjects. However, substantial inter-subject variability in human EEG could be an enduring obstacle for building a robust and capable EEG-based BCI from other individuals' data [90].

Our previous studies have shown that changes in EEG spectra are highly correlated with minute-scale fluctuations of a global level of drowsiness, indexed by the

sustained-attention performance [17][21][41]. Furthermore, this relationship is stable within individuals across sessions, but variable across individuals [17]. Thus, blindly training a BCI with all existing data from different individuals could deteriorate more than improve its performance. Fortunately, as the relationship between the EEG spectra and the drowsiness level are relatively stable across sessions within an individual, it might be possible to select informative data (or positive samples/sessions) from other individuals based on the EEG-drowsiness correlation seen in the pilot data from the test individual.

This study thus investigates the feasibility of transferring the knowledge of existing data to enhance the performance of EEG-based BCI. Specifically, this study proposes a framework of selective transfer learning (TL) to exploit a test subject's pilot session to select auxiliary models from other subjects to build a more accurate and robust drowsiness-detection BCI. The results of the proposed method are compared to that of a conventional within-subject cross-session validation approach in drowsiness detection and a routine, i.e., non-selective, TL.

A.2 Materials and Methods

A.2.1 Experiment and Participants

A lane-keeping driving task [117] was adopted to study the EEG correlates of participant's cognitive state. During the experiment, a participant was seated in a driving simulator and was instructed to steer the car back to the original cruising lane as quickly as possible once s/he realized the car was drifted from the cruising position (i.e., a lane-departure event). The lane-departure event was introduced randomly every 8-12 s after

the end of the previous event. Thirty-six voluntary participants with normal or corrected-to-normal vision participated in a total of 77 sessions of the lane-keeping driving task. These data were adopted from four different studies [19][40][50][118] in which participants performed the same lane-keeping driving task. The experiment was approved by the Institutional Review Board of the Veterans General Hospital, Taipei, Taiwan. All participants read and signed an informed consent form before the experiments. Fifteen subjects performed the driving task multiple times on different days, resulting in a total of 36 sessions. This study examined the feasibility of the proposed selective transfer learning framework (see below) on these sessions.

A.2.2 EEG Dataset and Preprocessing

This study used EEG data collected by a 32-channel Quik-Cap (Compumedical NeuroScan, Inc.) from electrodes placed according to the international 10-20 system, and referenced to the arithmetic mean of the left and right mastoids. The impedance of all electrodes was kept under 5k Ohm during the experiments. The EEG signals were recorded with 16-bit quantization level at the sampling rate of 500 Hz. The EEG data were first processed by a 1-50 Hz band-pass finite impulse response filter to remove low-frequency drifts and high-frequency artifacts. Severe artifacts or noise were then manually removed. The resultant EEG data were further down-sampled to 250 Hz before further analysis.

A.2.3 Estimation of Drowsiness Level

This study first defined the behavioral performance during the lane-keeping driving task based on the reaction time (RT) responded to randomly induced lane-departure events. That is the time interval before the onset of the lane-departure event and

the onset of steering wheel. For each session, the measured RT of each lane-departure trial was normalized according to the following equation:

$$\text{Normalized RT} = \begin{cases} 0 & , \tau \leq \tau_0 \\ (1 - e^{-(\tau-\tau_0)}) / (1 + e^{-(\tau-\tau_0)}) & , \tau > \tau_0 \end{cases}$$

where τ is the RT to a lane-departure event, and τ_0 is the alert reaction time, which is empirically defined by the median RTs of the 10% of all trials that had shortest RTs in the session. The resultant normalized RT ranged from zero (fully alert) to one (drowsiness). The drowsiness level was then derived from the average of the normalized RTs within a 90-second window before the onset of each trial under study.

A.2.4 EEG Feature Extraction

This study explored the relationship between the EEG activities and drowsiness level by correlating the EEG spectra with the putative drowsiness level. For each channel, a 256-point Welch's fast Fourier transform was applied to a 64-point moving window (zero-padded to 256 points) with an overlap of 52 points to calculate the spectral power with a frequency resolution of ~ 1 Hz. This study focused on the spectra between 0.98 and 30.3 Hz (30 frequency bins). The spectral power of each channel was then converted into a logarithmic scale. The resultant power spectra were then normalized by the baseline power that was calculated from the average power of the first 60 seconds of a session.

A.2.5 EEG-Based Drowsiness Regression Model

This study employed a typical linear regression model to assess the relationship between the EEG spectra and the drowsiness level for each session. Prior to building a model, a dimension-reduction procedure based on principal component analysis (PCA) was applied to the EEG spectra. PCA transferred the 900-dimension EEG spectra (30

channels \times 30 frequencies) into a set of principal components (PCs). Only a subset of PCs accounting for 80% of the data variance was retained and used for the regression analysis. The present study used the Pearson correlation coefficient between the actual and predicted RTs as a metric to evaluate the performance of drowsiness estimation.

A.2.6 Level of Session Generalizability

This study hypothesized that if the pilot session of an individual provides discriminative information between alertness and drowsiness for the session and for sessions from others, then the information from others might not add any value to improve the model based solely on the pilot session for the individual. Conversely, if the pilot session is not informative enough to model the drowsiness level as well as is not generalizable to predict the drowsiness level of sessions from others, then the model for this individual might benefit from the transfer learning procedure. That is, the individual's model can be improved by leveraging the models based on others' data to better estimate the drowsiness level of an unseen (test) session from the subject. To this end, it was imperative to characterize the extent of the generalizability of each session for each individual. This study thus defined a term, the level of session generalizability (LSG), that essentially accounts for both the performance of a given session and the performance of using that session to estimate the sessions from other subjects. The calculation of LSG is formularized as follows:

$$LSG_i = \frac{P(i, i) + \overline{P(i, \Phi(i))}}{P(j, j) + \overline{P(j, \Phi(j))}} \Big|_{j \in \Phi(i)}$$

where

$P(\mathbf{a}, \mathbf{b}) \equiv$ performance (Pearson correlation between actual and predicted RTs) of session a's model on session b

$\Phi(\mathbf{i}) \equiv$ assemble of indices of sessions from all other subjects of session i

$\overline{P(\mathbf{i}, \Phi(\mathbf{i}))}$ = the median performance of using session i's model on all other subjects' sessions

The LSG of a given session is the summation of its self-prediction performance and its prediction ability to other sessions with respect to the self-prediction and cross-session performance of other subjects' sessions. This study empirically separated the 36 sessions into high- and low-LSG groups with the threshold of LSG=1. That is, under our hypothesis, the pilot session with LSG<1 tended to benefit from the TL procedure to model the test session from the same individual. Otherwise, the TL is not recommended to augment the pilot model for the sessions with LSG>1.

A.2.7 Selecting Auxiliary Sessions for Transfer Learning

In order to study how many auxiliary sessions were required for a TL procedure to improve the performance of the pilot model, this study systematically incorporated more sessions from other subjects and compared their TL performance. Specifically, for a given pilot session, all of its auxiliary sessions (within-subject sessions were excluded) were ranked by their performance in estimating the drowsiness level of the pilot session. The models from top-ranked auxiliary sessions were recruited first. The output drowsiness level for an unseen session was determined by the mean of the predicted values of all N+1 sessions (N from other subjects, one from the pilot session).

A.2.8 Selective transfer Learning and Performance Evaluation

This study proposed a framework of selective transfer learning to test the posed hypothesis that the sessions with lower LSG could benefit from leveraging other subjects' models. Thus, only the subjects whose pilot sessions had low-LSG would leverage the models from others to build a TL-augmented model. The performance using the proposed selective transfer learning was evaluated and compared to those based on the within-subject cross-session validation, i.e., only using the pilot model from each individual to predict the unseen session (without TL) from the same individual, and routine (non-selective) TL validation, i.e., forcing all individuals to use TL-augmented approach.

A.3 Results

Figure A.1 shows the performance improvement with transfer learning as a function of the level of session generalizability. As can be seen, the TL improvement was found negatively correlated with the LSG values ($p=0.0004$). The sessions with lower LSG values tended to get improved more from the TL procedure that leveraged other subjects' sessions, which evidently supported our hypothesis.

Figure A.2 portrays the performance of the TL-augmented pilot sessions (with $LSG < 1$) as a function of the number of auxiliary sessions involved. The performance based on the within-subject cross-session validation (without TL) was also provided for comparison. Note that among the 36 pairs of pilot and test sessions, twenty pilot sessions were regarded as low generalizability and subject to this comparative study. In general, the TL-augmented pilot models (red solid line) significantly outperformed the performance based on the within-subject cross-session validation (gray line, without TL).

The TL-augmented performance rose steadily until 24 top-comparable auxiliary models from other subjects were included, but then started declining when adding more auxiliary models. This result suggested that naively pooling all auxiliary sessions together might not necessarily lead to better performance for a pilot model. Thus, selecting an optimal set of the auxiliary models for a pilot model was an imperative step to the success of transfer learning.

Figure A.3 shows the performance using three different approaches: the proposed selective transfer learning, routine transfer learning, and within-subject cross-session validation. Specifically, Figure A.3 (a) shows the comparative results along the individual sessions. As shown in Figure A.3 (a), in the high LSG group ($LSG > 1$) where the selective TL directly inherited the performance of within-subject validation (that is, no distinct TL improvement for these subjects). On the other side, the selective TL directly inherited the results from the TL-augmented models (red open circles and blue squares were completely overlapped for the $LSG < 1$ group 1). Figure A.3 (b) compares the average drowsiness-detection performances in high and low LSG sessions obtained by different approaches. TL was unable to improve the accuracy of drowsiness detection in the high LSG sessions, but could offer significant improvements for the low LSG sessions. The overall performance in Figure A.3 (c) suggested that the proposed selective TL could enhance the performance of drowsiness estimation.

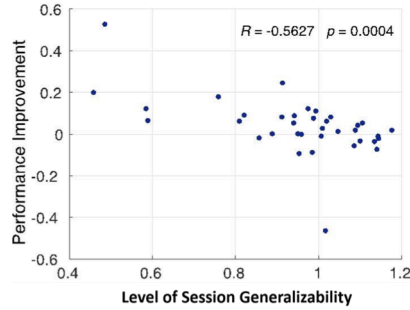


Figure A.1: The performance improvement with transfer learning as a function of the level of session generalizability (*LSG*). The significantly negative correlation implies that a pilot model with lower *LSG* value benefited more from applying transfer learning approach to estimate the drowsiness level.

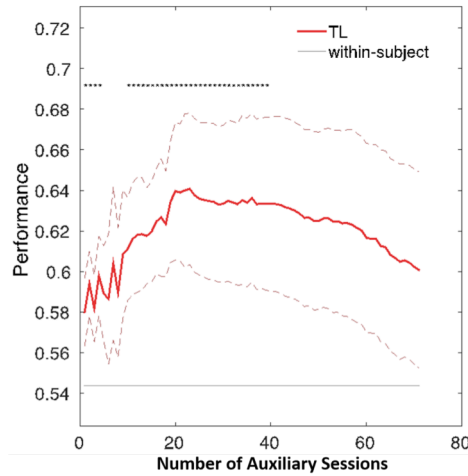


Figure A.2: The performances of TL-augmented sessions (with $LSG < 1$) as a function of the number of auxiliary sessions involved. The performance based on within-subject validation was also provided for comparison. Red bold line shows the mean of the TL performance for 20 low-*LSG* session pairs, whereas red dashed lines represent their standard errors. Gray line indicates the performance based on the within-subject validation (without TL). Asterisk indicates the significant difference between TL and within-subject performances assessed by a paired *t*-test ($p < 0.05$).

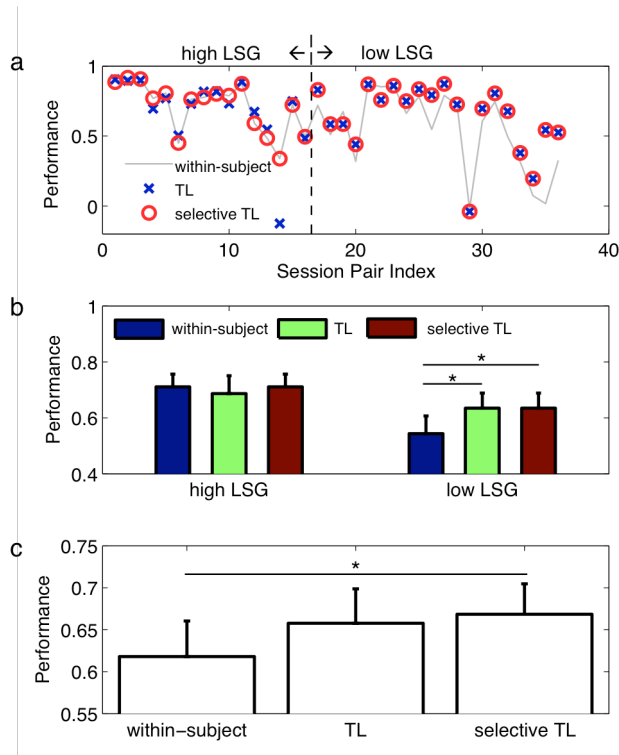


Figure A.3: The performance using the proposed selective TL, TL (non-selective), and within-subject cross-session validation. (a) presents the comparative results along the individual sessions. Sixteen session pairs were regarded as high *LSG*, whereas twenty sessions were categorized as low *LSG*. (b) compares three approaches separately in high and low *LSG* conditions. TL and selective TL both outperformed within-subject under low *LSG* condition (paired *t*-test, $p < 0.01$). (c) The selective TL showed consistently significant improvements for all 36 sessions as compared to the with-subject and TL methods using a paired *t*-test ($p < 0.01$).

A.4 Discussions and Conclusion

This study investigated the feasibility of leveraging existing data from other subjects to improve the performance of a drowsiness-detection BCI. The study results showed that exploiting data from other subjects for an individual was not always favorable for estimating the level of drowsiness in a new session for the same individual. As shown in Figure A.1, transfer learning could sometimes deteriorate more than improve the within-subject BCI performance. The results of this study also showed that a

pilot session with high LSG might not be able to take advantage of other subjects' data using the transfer learning method implemented in this paper. Therefore, it might be necessary to formulate a strategy to selectively apply transfer learning under different circumstances.

To appropriately select auxiliary data, this study ranked each session from other subjects by the performance of each session's model testing against the other subject's data. The obtained empirical results showed that the ranking method was effective for selecting informative auxiliary data (c.f. Figure A.2), where the transfer learning performance was improved even using only one extra session, and was gradually increased until using ~24 sessions. Figure A.3 shows a comparison study among three approaches: routine TL, selective TL and no-TL. The selective TL evidently outperformed others.

In summary, this study proposed a framework to effectively leverage a large amount of training data from other subjects and a small amount of subject-specific pilot data to improve BCI performance. This framework can be useful to obtain good BCI performance when collecting a sufficient amount of subject-specific pilot data is difficult or impossible.

A.5 Acknowledgement

This section contains material partly from "Selective Transfer Learning for EEG-Based Drowsiness Detection" by Chun-Shu Wei, Yuan-Pin Lin, Yu-Te Wang, Tzyy-Ping Jung, Nima Bigdely-Shamlo, and Chin-Teng Lin, which appears in the *IEEE Conference on Systems, Man, and Cybernetics (SMC 2015)*. The dissertation author was the first

investigator and author of this paper. The material is copyright ©2015 by the Institute of Electrical and Electronics Engineers (IEEE).

APPENDIX B

EXPLORING THE EEG CORRELATES OF DROWSINESS WITH ROBUST PRINCIPAL COMPONENT ANALYSIS

Recent developments of brain-computer interfaces (BCIs) for driving drowsiness detection based on electroencephalogram (EEG) have made much progress. This study aims to leverage these new developments and explore the use of robust principal component analysis (RPCA) to extract informative EEG features associated with drowsiness. Study results showed that the RPCA decomposition could separate drowsiness-related EEG dynamics from the task-irrelevant spontaneous background activity, leading to more robust neural correlates of drowsiness as compared to the original EEG signals. This study will shed light on the development of a robust drowsiness-detection BCI system in real-world environments.

B.1 Background

The drowsiness has been known as a critical safety issue in vehicle driving. Such momentary drowsiness causes approximate 1.9 million drivers to fatal car accidents with injury or death [15]. Technologies that enable instant drowsiness detection and feedback delivery to rectify drivers from the occurrence of drowsiness are thus urgently required. For the past two decades, the noninvasive brain-sensing technology, namely

electroencephalogram (EEG), has been adopted for this purpose because of its high temporal resolution of brain signals allowing a prompt response to drowsiness. For example, studies have shown strong EEG correlates of behavioral drowsiness, including power spectra [17][19][20][65] and autoregressive features [119][120]. These EEG features could then be used to develop various on-line/off-line neuroergonomic systems for monitoring drowsiness, fatigue, and behavioral drowsiness in task performance [17][19][41][63][77][121]. It is believed that an effective computational approach that can further leverage EEG correlates of drowsiness is a crucial step for improving the practicability of BCI-based drowsiness detection system in real life, which is the main focus of this study.

Robust principal component analysis (RPCA) [122] has recently been shown to be able to separate task-relevant and sparse EEG dynamics from the spontaneous task-irrelevant background activity [123]. The study demonstrated that the RPCA could improve the characterization of emotion-related EEG patterns across different recording days, and in turn facilitate a more effective emotion-classification model. As such, the task-related EEG dynamics of interest could be extracted from the task-irrelevant spontaneous background activity using RPCA, and could alleviate the EEG variability across sessions [123]. Analogously, this study explores the applicability of the RPCA for assessing the EEG correlates of neurocognitive drowsiness during driving.

B.2 Materials and Methods

B.2.1 Experiment and EEG Recording

This proof-of-concept study employed an EEG dataset of eight subjects participating in a lane-keeping driving task (LKT) in which EEG data and human driving behavior were simultaneously recorded [117]. The experiments were conducted in a virtual-reality-based driving simulator. Each subject drove on a straight highway scene during the night with artificial lane-deviation events introduced every 6-10 seconds. In each lane-deviation event, the car would randomly drift toward to left or right, and the subject was instructed to steer the car back to the cruising position as soon as possible. The duration from the onset of lane-deviant to the onset of steering movement was defined as the reaction time (RT), which indexed the extent of neurocognitive drowsiness. Longer RT indicated poor driving performance at the given moment. The experiment started in early afternoon when afternoon slump often occurred and thus maximized the opportunity of collecting neurocognitive drowsiness. The entire session of LKT lasted about 90 minutes, which was long enough to collect sufficient data under both alertness and drowsiness.

The EEG data were recorded by a 32-channel Quik-Cap electrode system (Compumedics Neuroscan, Inc.). Thirty Ag/AgCl electrodes were deployed according to the modified international 10-20 system, and two reference electrodes were placed upon left and right mastoids. The EEG signals were sampled with 16-bit quantization and 500 Hz sampling rate.

B.2.2 Experiment and EEG Recording

In this study, drowsiness refers to momentary unresponsiveness to the lane-deviation event in the LKT, and its level was quantitatively estimated based on RT. This study empirically defined the RT as alertness if its value was below the 5th percentile of the RTs across entire session for each session. In order to calibrate the individual differences in the distributions of RT values, the RTs of each individual was further normalized into a range of 0 to 1, defined as follows [121]:

$$DI = \max(0, (1 - e^{-a(\tau-\tau_0)})/(1 + e^{-a(\tau-\tau_0)}))$$

where τ is the RT of the given lane-departure event, and a is a constant set as 1 s^{-1} . The higher DI value is, the more momentary drowsiness a subject is showing. This study used correlation analysis to investigate the relationship between the EEG dynamics and the changes of RT.

B.2.3 EEG Data Processing

The 30-channel EEG signals referenced to the arithmetic average of left and right mastoid were first submitted to a band-pass finite impulse response filter (2 to 30 Hz) to eliminate DC drift and high-frequency noise including 60 Hz powerline noise. Trials contaminated by artifacts or noise were manually inspected and removed. Next, the filtered 30-channel EEG data were down-sampled to 250 Hz for analysis.

Previous studies [17][19] have reported significant EEG spectral correlates of RT in stereotype frequency bands, such as delta (1-4 Hz), theta (4-8 Hz), alpha (8-13 Hz), and beta (13-30 Hz) bands. This study thus examined the impact of RPCA processing on EEG spectral time series in the same EEG frequency bands. To assess the associations between EEG dynamics and cognitive drowsiness, this study first calculated the band

power (logarithmic signal variance) of each channel within a 3-second window before the onsets of each lane-deviation events, and then correlated that with the corresponding RT values.

B.2.4 Robust Principal Component Analysis

The applicability of the RPCA [120] has been demonstrated in effectively separating emotion-relevant and sparse EEG dynamics from the spontaneous task-irrelevant background activity. This study employed RPCA for assessing the EEG correlates of drowsiness during driving. The RPCA mathematically decomposes multi-channel EEG signals, $X \in \mathbf{R}^{m \times n}$ (m: number of attributes, n: number of observations), into a sparse matrix, S , and a low-rank matrix, L , followed by $X = S + L$, which can be efficiently solved by a tractable convex optimization proposed in [13]:

$$\mathbf{min}_{S^+, L^+} \lambda \|S^+\|_1 + \|L^+\|_* \quad \text{subject to } X = S + L$$

where $\|\cdot\|_*$ denotes the matrix nuclear norm, i.e., the sum of singular values, $\|\cdot\|_1$ denotes the L1 norm, i.e., the sum of absolute values of matrix entries, S^+ is the optimized estimate of sparse component, L^+ is the optimized estimate of low-rank component, and λ is a positive regularizing parameter empirically defined as $\lambda = 1/\sqrt{\max(m, n)}$ [13]. This study formed the input matrix (m: number of electrodes \times number of time points in a 3-s epoch, n: number of epochs in a session) for each subject. The method of augmented Lagrange multipliers [124] was adopted to perform RPCA decomposition. After the RPCA decomposition, the correlation coefficients between the normalized RTs (the drowsiness index) and the EEG spectral features estimated separately from the original band-passed EEG signals, sparse component, and low-rank component were compared using a statistical assessment of Wilcoxon signed-rank test.

This study hypothesized that the sparse components, S , would profitably extract drowsiness-related EEG dynamics, and therefore would be more correlated with the RTs, compared to the low-rank components, L , and the original EEG signals, X .

B.3 Results and Discussion

Figure B.1 illustrates the time series of RT profiles before and after the proposed RT normalization in two representative subjects. The alert RT is set to 0.6 second to map the RT to the drowsiness index. When a RT value is close to the defined alert RT, the drowsiness index increases more linearly as RT increases, until it reaches to a plateau close to 1 as RT is 4 seconds or longer. This warping is based on an assumption that there is very little difference in the brain state between 4- and 10-second RT as the subject was unresponsive to lane-deviation events. As can be seen, before the RT normalization shown in Figure B.1 (b), S1 seemed to retain alert across the entire session, while S2 frequently behaved with drowsiness after 10 min driving. However, the drowsiness index after the RT normalization exhibited realistic fluctuations of drowsiness for both S1 and S2 in a 90-min driving task as shown in Figure B.1 (c).

Figure B.2 explores the statistical significance of the correlations ($\log p$ -value) between RTs and band power at different scalp locations using the (the 1st row) band-passed EEG signals, (the 2nd row) sparse components, and (the 3rd row) low-rank components. Brightness in gray-scaled topographies represents the correlation was statistically significant (a strong correlation) between the band power and RTs. The 4th (5th) row plots the differences of p -values between the 1st and the 2nd (3rd) rows. The red squares mark the channels whose correlations between the band power and RTs were

significantly enhanced in terms of the p-value over using the original EEG band power. Specifically, the ‘Original’ scalp map exhibited strong correlations in frontal delta, moderate correlations in frontal theta, and parietal-occipital theta and alpha, which were somewhat in line with previous studies [17][19]. The sparse components obtained by RPCA enhanced the extents of the correlations between the EEG power and RTs at several channels (marked in red), compared to the original scalp-EEG band power. The augmentations in the highlighted channels (see the 4th row, Sparse - Original) were statistically significant. In contrast, the low-rank component did not provide any improvement in the correlations between EEG power and RTs (see the bottom row, Low-rank – Original).

Figure B.3 plots the comparative correlation coefficients between band power and RTs using the band-passed EEG signals, sparse components, and low-rank components at four representative locations, including Fz, Cz, Pz, and Oz. The improvements of spectrum-RT correlation could be found by the enhancement in correlation coefficients between RTs and Fz delta, Cz delta and theta, Pz delta, theta, and alpha, and Oz delta, theta, and alpha power. In particular, the highest correlation could be obtained at Oz (alpha power) using the original band-passed EEG signal, where the sparse component further strengthened this correlation. Subtle discrepancy in statistical testing results could be found as compared to Figure B.2 due to the different measurements (logarithmic p-values and correlation coefficients) that were used in the statistical test. For instance, there is significant enhancement at F4 delta (see the red dot at delta, 1st column & 4th row in Figure B.2), but no significance at the nearby Fz delta. However, the correlation coefficient was significantly enhanced at Fz delta (see the top left of Figure B.3). Note

that the sparse components generated features with higher correlations for most of the comparative conditions, which was consistent with the inference from the results shown in Figure B.2. The comparison of correlation coefficients suggests that sparse component can enhance the discriminative power of drowsiness-related EEG features.

The above findings evidently proved the posed hypothesis that the sparse EEG signals obtained by RPCA can profitably extract drowsiness-related EEG dynamics, and therefore carry more informative EEG spectral features accounting for behavioral drowsiness. In this preliminary proof-of-concept study, with such an improvement in feature extraction for EEG correlates of drowsiness, we believe that RPCA could boost the performance of a drowsiness detecting system.

While previous studies have applied independent component analysis (ICA) to extract highly informative EEG correlates of drowsiness [19][41], a quantitative comparison between RPCA, ICA, and other related approaches on enhancing the quality of EEG features would be of interest to the researchers in this field and a natural next step of this study. Future work will also study to what extent the RPCA-enhanced EEG spectral correlates of drowsiness can improve the performance of drowsiness detection, which will increase the practicability of BCI-based drowsiness detection system in real life.

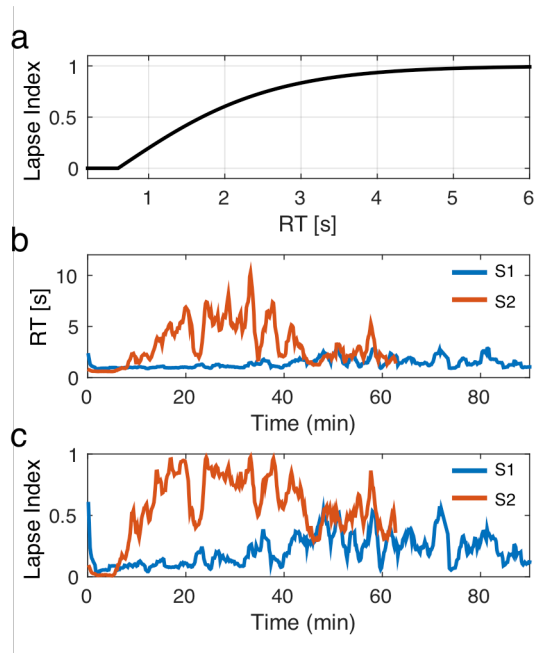


Figure B.1: Time series of RTs before and after RT normalization in two representative subjects. (a) the conversion from RT to the proposed lapse index with alert RT = 0.6 s. (b) the time series of original RTs in Subjects S1 and S2, and (c) the time series of the lapse index after RT normalization.

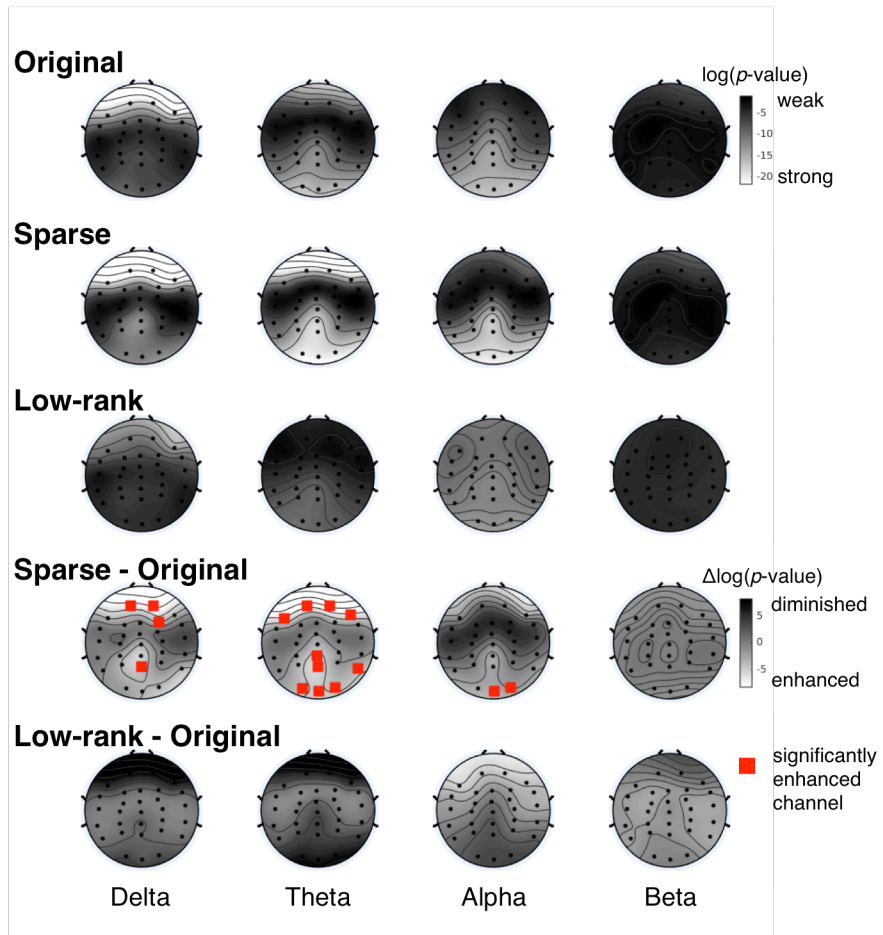


Figure B.2: The statistical significance of the correlations ($\log p$ -value) between RTs and band power using (from the top) the band-passed EEG signals (original), sparse components, and low-rank components at different scalp locations. The correlation intensity was estimated by logarithmic p -value from correlation analysis. Brightness in the gray-scaled topographies represents a strong correlation between the EEG band power and RTs. (the 4th row) Sparse - Original (the 5th row, Low-rank - Original) compares the significance of correlations between sparse (low-rank) and the original spectra. The red squares mark the channels with not only strong correlation ($\log(p) < -11$), but also significant increases from that of original EEG band power ($p < 0.05$).

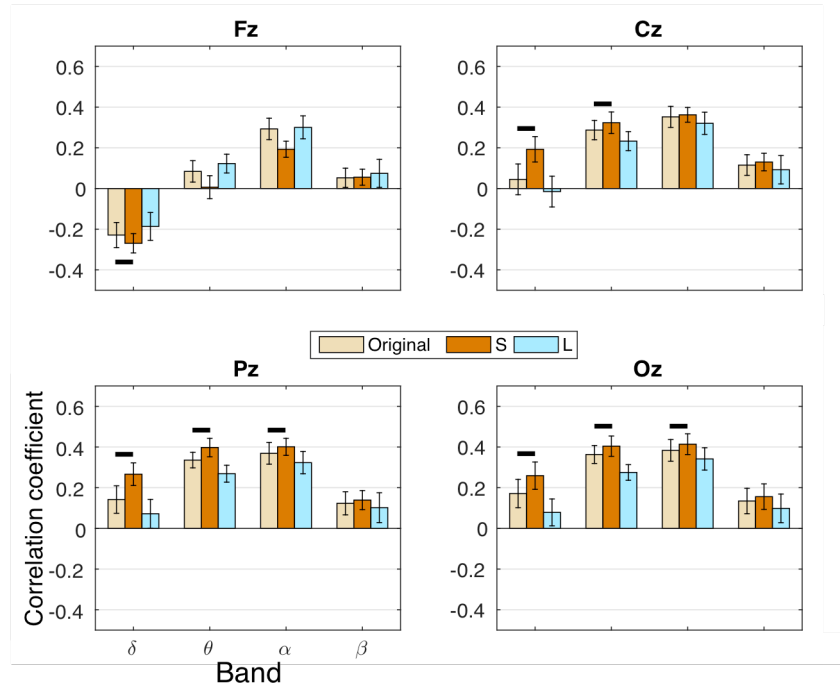


Figure B.3: The average correlation coefficients between band power and RTs at four representative scalp locations (Fz, Cz, Pz, and Oz) using the band-passed EEG signals (Original), sparse components (S), and low-rank components (L). Black bars indicate significant increase (either positive or negative) in correlation coefficient ($p < 0.05$) comparing S to Original.

B.4 Conclusion

The present study empirically demonstrated the efficacy of RPCA for enhancing EEG correlates of drowsiness. Study results suggested that the RPCA could be used as a pre-processing step to extract the drowsiness-related EEG dynamics of interest from the spontaneous background activity, leading to a more robust drowsiness-detection BCI in real-world environments.

B.5 Acknowledgement

This section contains material partly from “Exploring the EEG Correlates of Neurocognitive Lapse with Robust Principal Component Analysis” by Chun-Shu Wei, Yuan-Pin Lin, and Tzyy-Ping Jung, which appears in *the Proceedings of International Conference on Augmented Cognition, 2016*. The dissertation author was the first investigator and author of this paper. The material is copyright ©2016 by Springer International Publishing AG.

BIBLIOGRAPHY

- [1] J. R. Wolpaw, N. Birbaumer, W. J. Heetderks, D. J. McFarland, P. H. Peckham, G. Schalk, E. Donchin, L. A. Quatrano, C. J. Robinson, and T. M. Vaughan, "Brain-computer interface technology: a review of the first international meeting," *IEEE Transactions on Rehabilitation Engineering*, vol. 8, no. 2, pp. 164–173, Jun. 2000.
- [2] J. R. Wolpaw, N. Birbaumer, D. J. McFarland, G. Pfurtscheller, and T. M. Vaughan, "Brain–computer interfaces for communication and control," *Clinical Neurophysiology*, vol. 113, no. 6, pp. 767–791, Jun. 2002.
- [3] G. Pfurtscheller, C. Neuper, G. R. Muller, B. Obermaier, G. Krausz, A. Schlogl, R. Scherer, B. Graimann, C. Keinrath, D. Skliris, M. Wortz, G. Supp, and C. Schrank, "Graz-BCI: state of the art and clinical applications," *IEEE Transactions on Neural Systems and Rehabilitation Engineering*, vol. 11, no. 2, pp. 1–4, Jun. 2003.
- [4] S. Koike, Y. Nishimura, R. Takizawa, N. Yahata, and K. Kasai, "Near-Infrared Spectroscopy in Schizophrenia: A Possible Biomarker for Predicting Clinical Outcome and Treatment Response," *Front Psychiatry*, vol. 4, Nov. 2013.
- [5] R. K. Mehta and R. Parasuraman, "Neuroergonomics: a review of applications to physical and cognitive work," *Front Hum Neurosci*, vol. 7, Dec. 2013.
- [6] T. J. Sejnowski, P. S. Churchland, and J. A. Movshon, "Putting big data to good use in neuroscience," *Nat Neurosci*, vol. 17, no. 11, pp. 1440–1441, Nov. 2014.
- [7] M. Kaper, P. Meinicke, U. Grossekhoefer, T. Lingner, and H. Ritter, "BCI competition 2003-data set IIB: support vector machines for the P300 speller paradigm," *IEEE Transactions on Biomedical Engineering*, vol. 51, no. 6, pp. 1073–1076, Jun. 2004.
- [8] X. Chen, Y. Wang, M. Nakanishi, X. Gao, T.-P. Jung, and S. Gao, "High-speed spelling with a noninvasive brain–computer interface," *PNAS*, p. 201508080, Oct. 2015.
- [9] G. E. Fabiani, D. J. McFarland, J. R. Wolpaw, and G. Pfurtscheller, "Conversion of EEG activity into cursor movement by a brain-computer interface (BCI)," *IEEE Transactions on Neural Systems and Rehabilitation Engineering*, vol. 12, no. 3, pp. 331–338, Sep. 2004.
- [10] J. R. Millan and J. Mourino, "Asynchronous BCI and local neural classifiers: an overview of the adaptive brain interface project," *IEEE Transactions on Neural Systems and Rehabilitation Engineering*, vol. 11, no. 2, pp. 159–161, Jun. 2003.

- [11] K. LaFleur, K. Cassady, A. Doud, K. Shades, E. Rogin, and B. He, “Quadcopter control in three-dimensional space using a noninvasive motor imagery-based brain–computer interface,” *J. Neural Eng.*, vol. 10, no. 4, p. 046003, 2013.
- [12] A. H. Do, P. T. Wang, C. E. King, S. N. Chun, and Z. Nenadic, “Brain-computer interface controlled robotic gait orthosis,” *Journal of NeuroEngineering and Rehabilitation*, vol. 10, p. 111, Dec. 2013.
- [13] A. R. C. Donat, S. Shokur, E. Morya, D. S. F. Campos, R. C. Muioli, C. M. Gitti, P. B. Augusto, S. Tripodi, C. G. Pires, G. A. Pereira, F. L. Brasil, S. Gallo, A. A. Lin, A. K. Takigami, M. A. Aratanha, S. Joshi, H. Bleuler, G. Cheng, A. Rudolph, and M. A. L. Nicolelis, “Long-Term Training with a Brain-Machine Interface-Based Gait Protocol Induces Partial Neurological Recovery in Paraplegic Patients,” *Scientific Reports*, vol. 6, p. srep30383, Aug. 2016.
- [14] M. Teplan, “Fundamentals of EEG Measurement,” in *Measurement Science Review, Volume 2, Section*, 2002.
- [15] NHTSA, “Drowsy Driving.” [Online]. Available: <https://www.nhtsa.gov/risky-driving/drowsy-driving>. [Accessed: 26-Sep-2017].
- [16] S. Makeig and M. Inlow, “Lapse in alertness: coherence of fluctuations in performance and EEG spectrum,” *Electroencephalography and Clinical Neurophysiology*, vol. 86, no. 1, pp. 23–35, Jan. 1993.
- [17] T.-P. Jung, S. Makeig, M. Stensmo, and T. J. Sejnowski, “Estimating alertness from the EEG power spectrum,” *IEEE Transactions on Biomedical Engineering*, vol. 44, no. 1, pp. 60–69, Jan. 1997.
- [18] P. Parikh and E. Micheli-Tzanakou, “Detecting drowsiness while driving using wavelet transform,” in *Bioengineering Conference, 2004. Proceedings of the IEEE 30th Annual Northeast*, 2004, pp. 79–80.
- [19] C.-T. Lin, R.-C. Wu, S.-F. Liang, W.-H. Chao, Y.-J. Chen, and T.-P. Jung, “EEG-based drowsiness estimation for safety driving using independent component analysis,” *IEEE Transactions on Circuits and Systems I: Regular Papers*, vol. 52, no. 12, pp. 2726–2738, Dec. 2005.
- [20] P. R. Davidson, R. D. Jones, and M. T. R. Peiris, “EEG-Based Lapse Detection With High Temporal Resolution,” *IEEE Transactions on Biomedical Engineering*, vol. 54, no. 5, pp. 832–839, May 2007.
- [21] C. T. Lin, L. D. Liao, Y. H. Liu, I. J. Wang, B. S. Lin, and J. Y. Chang, “Novel Dry Polymer Foam Electrodes for Long-Term EEG Measurement,” *IEEE Transactions on Biomedical Engineering*, vol. 58, no. 5, pp. 1200–1207, May 2011.

- [22] C. Grozea, C. D. Voinescu, and S. Fazli, “Bristle-sensors—low-cost flexible passive dry EEG electrodes for neurofeedback and BCI applications,” *J. Neural Eng.*, vol. 8, no. 2, p. 025008, 2011.
- [23] Y. M. Chi, Y.-T. Wang, Y. Wang, C. Maier, T.-P. Jung, and G. Cauwenberghs, “Dry and Noncontact EEG Sensors for Mobile Brain-Computer Interfaces,” *IEEE Transactions on Neural Systems and Rehabilitation Engineering*, vol. 20, no. 2, pp. 228–235, Mar. 2012.
- [24] Y.-H. Chen, M. O. de Beeck, L. Vanderheyden, E. Carrette, V. Mihajlovic, K. Vanstreels, B. Grundlehner, S. Gadeyne, P. Boon, and C. Van Hoof, “Soft, Comfortable Polymer Dry Electrodes for High Quality ECG and EEG Recording,” *Sensors*, vol. 14, no. 12, pp. 23758–23780, Dec. 2014.
- [25] S. Xu, Y. Zhang, L. Jia, K. E. Mathewson, K. I. Jang, J. Kim, H. Fu, X. Huang, P. Chava, R. Wang, S. Bhole, L. Wang, Y. J. Na, Y. Guan, M. Flavin, Z. Han, Y. Huang, and J. A. Rogers, “Soft Microfluidic Assemblies of Sensors, Circuits, and Radios for the Skin,” *Science*, vol. 344, no. 6179, pp. 70–74, Apr. 2014.
- [26] J. J. S. Norton, D. S. Lee, J. W. Lee, W. Lee, O. Kwon, P. Won, S. Y. Jung, H. Cheng, J. W. Jeong, A. Akce, S. Umunna, I. Na, Y. H. Kwon, X. Q. Wang, Z. Liu, U. Paik, Y. Huang, T. Bretl, W. H. Yeo, and J. A. Rogers, “Soft, curved electrode systems capable of integration on the auricle as a persistent brain–computer interface,” *PNAS*, vol. 112, no. 13, pp. 3920–3925, Mar. 2015.
- [27] J. Gu and R. Kanai, “What contributes to individual differences in brain structure?,” *Front. Hum. Neurosci.*, vol. 8, p. 262, 2014.
- [28] H. Morioka, A. Kanemura, J. Hirayama, M. Shikauchi, T. Ogawa, S. Ikeda, M. Kawanabe, and S. Ishii, “Learning a common dictionary for subject-transfer decoding with resting calibration,” *NeuroImage*, vol. 111, pp. 167–178, May 2015.
- [29] V. Jayaram, M. Alamgir, Y. Altun, B. Scholkopf, and M. Grosse-Wentrup, “Transfer Learning in Brain-Computer Interfaces,” *IEEE Computational Intelligence Magazine*, vol. 11, no. 1, pp. 20–31, Feb. 2016.
- [30] S. Fazli, F. Popescu, M. Danóczy, B. Blankertz, K.-R. Müller, and C. Grozea, “Subject-independent mental state classification in single trials,” *Neural Networks*, vol. 22, no. 9, pp. 1305–1312, Nov. 2009.
- [31] B. Reuderink, J. Farquhar, M. Poel, and A. Nijholt, “A subject-independent brain-computer interface based on smoothed, second-order baselining,” in *2011 Annual International Conference of the IEEE Engineering in Medicine and Biology Society*, 2011, pp. 4600–4604.

- [32] W. Tu and S. Sun, “A subject transfer framework for EEG classification,” *Neurocomputing*, vol. 82, pp. 109–116, Apr. 2012.
- [33] W. Samek, M. Kawanabe, and K. R. Müller, “Divergence-Based Framework for Common Spatial Patterns Algorithms,” *IEEE Reviews in Biomedical Engineering*, vol. 7, pp. 50–72, 2014.
- [34] F. Lotte, “Signal Processing Approaches to Minimize or Suppress Calibration Time in Oscillatory Activity-Based Brain-Computer Interfaces,” *Proceedings of the IEEE*, vol. 103, no. 6, pp. 871–890, Jun. 2015.
- [35] I. Tavor, O. P. Jones, R. B. Mars, S. M. Smith, T. E. Behrens, and S. Jbabdi, “Task-free MRI predicts individual differences in brain activity during task performance,” *Science*, vol. 352, no. 6282, pp. 216–220, Apr. 2016.
- [36] E. M. Gordon, T. O. Laumann, B. Adeyemo, A. W. Gilmore, S. M. Nelson, N. U. F. Dosenbach, and S. E. Petersen, “Individual-specific features of brain systems identified with resting state functional correlations,” *NeuroImage*, vol. 146, pp. 918–939, Feb. 2017.
- [37] M. T. R. Peiris, R. D. Jones, P. R. Davidson, G. J. Carroll, and P. J. Bones, “Frequent lapses of responsiveness during an extended visuomotor tracking task in non-sleep-deprived subjects,” *J Sleep Res*, vol. 15, no. 3, pp. 291–300, Sep. 2006.
- [38] R.-S. Huang, T.-P. Jung, A. Delorme, and S. Makeig, “Tonic and phasic electroencephalographic dynamics during continuous compensatory tracking,” *NeuroImage*, vol. 39, no. 4, pp. 1896–1909, Feb. 2008.
- [39] C. T. Lin, K. C. Huang, C. F. Chao, J. A. Chen, T. W. Chiu, L. W. Ko, and T. P. Jung, “Tonic and phasic EEG and behavioral changes induced by arousing feedback,” *NeuroImage*, vol. 52, no. 2, pp. 633–642, 2010.
- [40] C.-H. Chuang, L.-W. Ko, T.-P. Jung, and C.-T. Lin, “Kinesthesia in a sustained-attention driving task,” *NeuroImage*, vol. 91, pp. 187–202, May 2014.
- [41] C.-H. Chuang, L.-W. Ko, Y.-P. Lin, T.-P. Jung, and C.-T. Lin, “Independent Component Ensemble of EEG for Brain-Computer Interface,” *IEEE Transactions on Neural Systems and Rehabilitation Engineering*, vol. 22, no. 2, pp. 230–238, Mar. 2014.
- [42] C.-T. Lin, C. H. Chuang, S. Kerick, T. Mullen, T. P. Jung, L. W. Ko, S. A. Chen, J. T. King, K. McDowell, “Mind-Wandering Tends to Occur under Low Perceptual Demands during Driving,” *Sci Rep*, vol. 6, Feb. 2016.
- [43] C. S. Wei, Y. P. Lin, Y. T. Wang, C. T. Lin, and T. P. Jung, “Transfer learning with large-scale data in brain-computer interfaces,” in *2016 38th Annual*

- International Conference of the IEEE Engineering in Medicine and Biology Society (EMBC)*, 2016, pp. 4666–4669.
- [44] T. Mullen, C. Kothe, Y. M. Chi, A. Ojeda, T. Kerth, S. Makeig, G. Cauwenberghs, and T. P. Jung, “Real-time modeling and 3D visualization of source dynamics and connectivity using wearable EEG,” in *2013 35th Annual International Conference of the IEEE Engineering in Medicine and Biology Society (EMBC)*, 2013, pp. 2184–2187.
- [45] A. Delorme and S. Makeig, “EEGLAB: an open source toolbox for analysis of single-trial EEG dynamics including independent component analysis,” *J. Neurosci. Methods*, vol. 134, no. 1, pp. 9–21, Mar. 2004.
- [46] M. B. Eisen, P. T. Spellman, P. O. Brown, and D. Botstein, “Cluster analysis and display of genome-wide expression patterns,” *PNAS*, vol. 95, no. 25, pp. 14863–14868, Dec. 1998.
- [47] W. F. Baaré, H. E. Hulshoff Pol, D. I. Boomsma, D. Posthuma, E. J. de Geus, H. G. Schnack, N. E. van Haren, C. J. van Oel, and R. S. Kahn, “Quantitative genetic modeling of variation in human brain morphology,” *Cereb. Cortex*, vol. 11, no. 9, pp. 816–824, Sep. 2001.
- [48] A. Y. Kaplan, A. A. Fingelkurts, A. A. Fingelkurts, S. V. Borisov, and B. S. Darkhovsky, “Nonstationary nature of the brain activity as revealed by EEG/MEG: Methodological, practical and conceptual challenges,” *Signal Processing*, vol. 85, no. 11, pp. 2190–2212, Nov. 2005.
- [49] I. Dinstein, D. J. Heeger, and M. Behrmann, “Neural variability: friend or foe?,” *Trends in Cognitive Sciences*, vol. 19, no. 6, pp. 322–328, Jun. 2015.
- [50] N. R. Pal, C. Y. Chuang, L. W. Ko, C. F. Chao, T. P. Jung, S. F. Liang, and C. T. Lin, “EEG-Based Subject- and Session-independent Drowsiness Detection: An Unsupervised Approach,” *EURASIP Journal on Advances in Signal Processing*, vol. 2008, no. 1, p. 519480, Nov. 2008.
- [51] R. R. Johnson, D. P. Popovic, R. E. Olmstead, M. Stikic, D. J. Levendowski, and C. Berka, “Drowsiness/alertness algorithm development and validation using synchronized EEG and cognitive performance to individualize a generalized model,” *Biological Psychology*, vol. 87, no. 2, pp. 241–250, 2011.
- [52] M. M. Moore, “Real-world applications for brain-computer interface technology,” *IEEE Transactions on Neural Systems and Rehabilitation Engineering*, vol. 11, no. 2, pp. 162–165, Jun. 2003.

- [53] B. Z. Allison, E. W. Wolpaw, and J. R. Wolpaw, "Brain-computer interface systems: progress and prospects," *Expert Review of Medical Devices*, vol. 4, no. 4, pp. 463–474, Jul. 2007.
- [54] J. B. F. Van Erp, F. Lotte, and M. Tangermann, "Brain-Computer Interfaces: Beyond Medical Applications," *Computer -IEEE Computer Society-*, vol. 45, no. 4, pp. 26–34, Apr. 2012.
- [55] K. McDowell, C. T. Lin, K. S. Oie, T. P. Jung, S. Gordon, K. W. Whitaker, S. Y. Li, S. W. Lu, and W. D. Hairston, "Real-World Neuroimaging Technologies," *IEEE Access*, vol. 1, pp. 131–149, 2013.
- [56] C. Grozea, C. D. Voinescu, and S. Fazli, "Bristle-sensors—low-cost flexible passive dry EEG electrodes for neurofeedback and BCI applications," *J. Neural Eng.*, vol. 8, no. 2, p. 025008, 2011.
- [57] C. T. Lin, L. D. Liao, Y. H. Liu, I. J. Wang, B. S. Lin, and J. Y. Chang, "Novel Dry Polymer Foam Electrodes for Long-Term EEG Measurement," *IEEE Transactions on Biomedical Engineering*, vol. 58, no. 5, pp. 1200–1207, May 2011.
- [58] Y. M. Chi, Y.-T. Wang, Y. Wang, C. Maier, T.-P. Jung, and G. Cauwenberghs, "Dry and Noncontact EEG Sensors for Mobile Brain-Computer Interfaces," *IEEE Transactions on Neural Systems and Rehabilitation Engineering*, vol. 20, no. 2, pp. 228–235, Mar. 2012.
- [59] P. Kidmose, D. Looney, M. Ungstrup, M. L. Rank, and D. P. Mandic, "A Study of Evoked Potentials From Ear-EEG," *IEEE Transactions on Biomedical Engineering*, vol. 60, no. 10, pp. 2824–2830, Oct. 2013.
- [60] S. Debener, R. Emkes, M. D. Vos, and M. Bleichner, "Unobtrusive ambulatory EEG using a smartphone and flexible printed electrodes around the ear," *Scientific Reports*, vol. 5, p. 16743, Nov. 2015.
- [61] H. T. Hsu, I. H. Lee, H. T. Tsai, H. C. Chang, K. K. Shyu, C. C. Hsu, H. H. Chang, T. K. Yeh, C. Y. Chang, and P. L. Lee, "Evaluate the Feasibility of Using Frontal SSVEP to Implement an SSVEP-Based BCI in Young, Elderly and ALS Groups," *IEEE Transactions on Neural Systems and Rehabilitation Engineering*, vol. 24, no. 5, pp. 603–615, May 2016.
- [62] Y. T. Wang, M. Nakanishi, Y. Wang, C. S. Wei, C. K. Cheng, and T. P. Jung, "An Online Brain-Computer Interface Based on SSVEPs Measured from Non-Hair-Bearing Areas," *IEEE Transactions on Neural Systems and Rehabilitation Engineering*, vol. PP, no. 99, pp. 1–1, 2016.

- [63] C.-S. Wei, Y.-T. Wang, C.-T. Lin, and T.-P. Jung, "Toward non-hair-bearing brain-computer interfaces for neurocognitive lapse detection," in *2015 37th Annual International Conference of the IEEE Engineering in Medicine and Biology Society (EMBC)*, 2015, pp. 6638–6641.
- [64] C. Kothe, "The Artifact Subspace Reconstruction method," 2013. [Online]. Available: <https://sccn.ucsd.edu/eeglab/plugins/ASR.pdf>. [Accessed: 17-Jul-2017].
- [65] S. K. L. Lal, A. Craig, P. Boord, L. Kirkup, and H. Nguyen, "Development of an algorithm for an EEG-based driver fatigue countermeasure," *Journal of Safety Research*, vol. 34, no. 3, pp. 321–328, Aug. 2003.
- [66] R. A. Fisher, "The Use of Multiple Measurements in Taxonomic Problems," *Annals of Eugenics*, vol. 7, no. 2, pp. 179–188, Sep. 1936.
- [67] H.-J. Hwang, S. Kim, S. Choi, and C.-H. Im, "EEG-Based Brain-Computer Interfaces: A Thorough Literature Survey," *International Journal of Human-Computer Interaction*, vol. 29, no. 12, pp. 814–826, Dec. 2013.
- [68] F. Lotte, M. Congedo, A. Lécuyer, F. Lamarche, and B. Arnaldi, "A review of classification algorithms for EEG-based brain-computer interfaces.," *Journal of neural engineering*, vol. 4, no. 2, 2007.
- [69] D. J. McFarland, C. W. Anderson, K.-R. Müller, A. Schlögl, and D. J. Krusienski, "BCI Meeting 2005--workshop on BCI signal processing: feature extraction and translation," *IEEE Trans Neural Syst Rehabil Eng*, vol. 14, no. 2, pp. 135–138, Jun. 2006.
- [70] C.-C. Chang and C.-J. Lin, "LIBSVM: A Library for Support Vector Machines," *ACM Trans. Intell. Syst. Technol.*, vol. 2, no. 3, p. 27:1–27:27, May 2011.
- [71] C. J. C. Burges, "A Tutorial on Support Vector Machines for Pattern Recognition," *Data Mining and Knowledge Discovery*, vol. 2, no. 2, pp. 121–167, 1998.
- [72] R. Meier, H. Dittrich, A. Schulze-Bonhage, and A. Aertsen, "Detecting epileptic seizures in long-term human EEG: a new approach to automatic online and real-time detection and classification of polymorphic seizure patterns," *J Clin Neurophysiol*, vol. 25, no. 3, pp. 119–131, Jun. 2008.
- [73] Y. Liu, O. Sourina, and M. K. Nguyen, "Real-Time EEG-Based Human Emotion Recognition and Visualization," in *2010 International Conference on Cyberworlds*, 2010, pp. 262–269.
- [74] Q. Wang and O. Sourina, "Real-Time Mental Arithmetic Task Recognition From EEG Signals," *IEEE Transactions on Neural Systems and Rehabilitation Engineering*, vol. 21, no. 2, pp. 225–232, Mar. 2013.

- [75] J.-R. Duann, P.-C. Chen, L.-W. Ko, R.-S. Huang, T.-P. Jung, and C.-T. Lin, "Detecting Frontal EEG Activities with Forehead Electrodes," in *Foundations of Augmented Cognition. Neuroergonomics and Operational Neuroscience*, D. D. Schmorrow, I. V. Estabrooke, and M. Grootjen, Eds. Springer Berlin Heidelberg, 2009, pp. 373–379.
- [76] J. Onton, M. Westerfield, J. Townsend, and S. Makeig, "Imaging human EEG dynamics using independent component analysis," *Neuroscience & Biobehavioral Reviews*, vol. 30, no. 6, pp. 808–822, 2006.
- [77] Y.-T. Wang, K. C. Huang, C. S. Wei, T. Y. Huang, L. W. Ko, C. T. Lin, C. K. Cheng, and T. P. Jung, "Developing an EEG-based on-line closed-loop lapse detection and mitigation system," *Front Neurosci*, vol. 8, p. 321, 2014.
- [78] B. J. Lance, S. E. Kerick, A. J. Ries, K. S. Oie, and K. McDowell, "Brain-Computer Interface Technologies in the Coming Decades," *Proceedings of the IEEE*, vol. 100, no. Special Centennial Issue, pp. 1585–1599, May 2012.
- [79] "EEG Headsets | NeuroSky Store." [Online]. Available: <http://store.neurosky.com/>. [Accessed: 22-Sep-2016].
- [80] "Muse – Muse: the brain sensing headband." [Online]. Available: http://store.choosemuse.com/products/muse?_ga=1.40886502.570081481.1474579055. [Accessed: 22-Sep-2016].
- [81] "EMOTIV EPOC+ 14 Channel Mobile EEG - Emotiv." [Online]. Available: <https://www.emotiv.com/product/emotiv-epoc-14-channel-mobile-eeq/>. [Accessed: 22-Sep-2016].
- [82] G. Bin, X. Gao, Z. Yan, B. Hong, and S. Gao, "An online multi-channel SSVEP-based brain-computer interface using a canonical correlation analysis method," *J Neural Eng*, vol. 6, no. 4, p. 046002, Aug. 2009.
- [83] C.-S. Wei, Y.-P. Lin, Y. Wang, Y.-T. Wang, and T.-P. Jung, "Detection of steady-state visual-evoked potential using differential canonical correlation analysis," in *2013 6th International IEEE/EMBS Conference on Neural Engineering (NER)*, 2013, pp. 57–60.
- [84] P.-J. Kindermans, M. Tangermann, K.-R. Müller, and B. Schrauwen, "Integrating dynamic stopping, transfer learning and language models in an adaptive zero-training ERP speller," *J Neural Eng*, vol. 11, no. 3, p. 035005, Jun. 2014.
- [85] I. Käthner, A. Kübler, and S. Halder, "Rapid P300 brain-computer interface communication with a head-mounted display," *Front. Neurosci.*, vol. 9, 2015.

- [86] A. Kondacs and M. Szabó, “Long-term intra-individual variability of the background EEG in normals,” *Clinical Neurophysiology*, vol. 110, no. 10, pp. 1708–1716, Oct. 1999.
- [87] F. Lotte and C. Guan, “An Efficient P300-based Brain-Computer Interface with Minimal Calibration Time,” in *Assistive Machine Learning for People with Disabilities symposium (NIPS’09 Symposium)*, Vancouver, Canada, 2009.
- [88] S. Lu, C. Guan, and H. Zhang, “Unsupervised Brain Computer Interface Based on Intersubject Information and Online Adaptation,” *IEEE Transactions on Neural Systems and Rehabilitation Engineering*, vol. 17, no. 2, pp. 135–145, Apr. 2009.
- [89] D. Devlaminck, B. Wyns, M. Grosse-Wentrup, G. Otte, and P. Santens, “Multisubject Learning for Common Spatial Patterns in Motor-imagery BCI,” *Intell. Neuroscience*, vol. 2011, p. 8:8–8:8, Jan. 2011.
- [90] D. Wu, B. J. Lance, and T. D. Parsons, “Collaborative Filtering for Brain-Computer Interaction Using Transfer Learning and Active Class Selection,” *PLoS ONE*, vol. 8, no. 2, p. e56624, 21 2013.
- [91] H. Kang and S. Choi, “Bayesian common spatial patterns for multi-subject EEG classification,” *Neural Networks*, vol. 57, pp. 39–50, Sep. 2014.
- [92] S. Dalhoumi, G. Dray, and J. Montmain, “Knowledge Transfer for Reducing Calibration Time in Brain-Computer Interfacing,” in *2014 IEEE 26th International Conference on Tools with Artificial Intelligence (ICTAI)*, 2014, pp. 634–639.
- [93] M. Arvaneh, I. Robertson, and T. E. Ward, “Subject-to-subject adaptation to reduce calibration time in motor imagery-based brain-computer interface,” in *2014 36th Annual International Conference of the IEEE Engineering in Medicine and Biology Society (EMBC)*, 2014, pp. 6501–6504.
- [94] O. Friman, T. Luth, I. Volosyak, and A. Graser, “Spelling with Steady-State Visual Evoked Potentials,” in *2007 3rd International IEEE/EMBS Conference on Neural Engineering*, 2007, pp. 354–357.
- [95] S. J. Pan and Q. Yang, “A Survey on Transfer Learning,” *IEEE Transactions on Knowledge and Data Engineering*, vol. 22, no. 10, pp. 1345–1359, Oct. 2010.
- [96] A. Vuckovic, V. Radivojevic, A. C. N. Chen, and D. Popovic, “Automatic recognition of alertness and drowsiness from EEG by an artificial neural network,” *Medical Engineering & Physics*, vol. 24, no. 5, pp. 349–360, Jun. 2002.
- [97] N. Langer, E. J. Ho, L. M. Alexander, H. Y. Xu, R. K. Jozanovic, S. Henin, A. Petroni, S. Cohen, E. T. Marcelle, L. C. Parra, M. P. Milham, and S. P. Kelly, “A

- resource for assessing information processing in the developing brain using EEG and eye tracking,” *Sci Data*, vol. 4, Apr. 2017.
- [98] B. Blankertz, C. Sannelli, S. Halder, E. M. Hammer, A. Kubler, K. R. Muller, G. Curio, and T. Dickhaus, “Neurophysiological predictor of SMR-based BCI performance,” *NeuroImage*, vol. 51, no. 4, pp. 1303–1309, Jul. 2010.
- [99] Y. Wang, Y.-T. Wang, and T.-P. Jung, “Translation of EEG Spatial Filters from Resting to Motor Imagery Using Independent Component Analysis,” *PLoS ONE*, vol. 7, no. 5, p. e37665, 29 2012.
- [100] J. Fernandez-Vargas, H. U. Pfaff, F. B. Rodriguez, and P. Varona, “Assisted closed-loop optimization of SSVEP-BCI efficiency,” *Front. Neural Circuits*, vol. 7, 2013.
- [101] J. J. Williams, A. G. Rouse, S. Thongpang, J. C. Williams, and D. W. Moran, “Differentiating closed-loop cortical intention from rest: building an asynchronous electrocorticographic BCI,” *J. Neural Eng.*, vol. 10, no. 4, p. 046001, 2013.
- [102] Y. Zhang, P. Xu, D. Guo, and D. Yao, “Prediction of SSVEP-based BCI performance by the resting-state EEG network,” *J. Neural Eng.*, vol. 10, no. 6, p. 066017, Dec. 2013.
- [103] S. Makeig and T. P. Jung, “Changes in alertness are a principal component of variance in the EEG spectrum,” *Neuroreport*, vol. 7, no. 1, pp. 213–216, Dec. 1995.
- [104] A. J. Tomarken, R. J. Davidson, R. E. Wheeler, and L. Kinney, “Psychometric Properties of Resting Anterior EEG Asymmetry: Temporal Stability and Internal Consistency,” *Psychophysiology*, vol. 29, no. 5, pp. 576–592, Sep. 1992.
- [105] J. Buckelmüller, H.-P. Landolt, H. H. Stassen, and P. Achermann, “Trait-like individual differences in the human sleep electroencephalogram,” *Neuroscience*, vol. 138, no. 1, pp. 351–356, 2006.
- [106] A. Gupta, S. Parameswaran, and C.-H. Lee, “Classification of electroencephalography (EEG) signals for different mental activities using Kullback Leibler (KL) divergence,” in *2009 IEEE International Conference on Acoustics, Speech and Signal Processing*, 2009, pp. 1697–1700.
- [107] N. Sulaiman, M. N. Taib, S. Lias, Z. H. Murat, S. A. M. Aris, and N. H. A. Hamid, “Novel methods for stress features identification using EEG signals,” *International Journal of Simulation: Systems, Science and Technology*, vol. 12, no. 1, pp. 27–33, Feb. 2011.

- [108] R. K. Chaurasiya, N. D. Londhe, and S. Ghosh, “A Novel Weighted Edit Distance-Based Spelling Correction Approach for Improving the Reliability of Devanagari Script-Based P300 Speller System,” *IEEE Access*, vol. 4, pp. 8184–8198, 2016.
- [109] E. S. Finn, X. Shen, D. Scheinost, M. D. Rosenberg, J. Huang, M. M. Chun, X. Papademetris, and R. T. Constable, “Functional connectome fingerprinting: identifying individuals using patterns of brain connectivity,” *Nat Neurosci*, vol. 18, no. 11, pp. 1664–1671, Nov. 2015.
- [110] H. Laufs, K. Krakow, P. Sterzer, E. Eger, A. Beyerle, A. Salek-Haddadi, and A. Kleinschmidt, “Electroencephalographic signatures of attentional and cognitive default modes in spontaneous brain activity fluctuations at rest,” *PNAS*, vol. 100, no. 19, pp. 11053–11058, Sep. 2003.
- [111] D. Mantini, M. G. Perrucci, C. D. Gratta, G. L. Romani, and M. Corbetta, “Electrophysiological signatures of resting state networks in the human brain,” *PNAS*, vol. 104, no. 32, pp. 13170–13175, Aug. 2007.
- [112] Y. Meir-Hasson, S. Kinreich, I. Podlipsky, T. Hendler, and N. Intrator, “An EEG Finger-Print of fMRI deep regional activation,” *NeuroImage*, vol. 102, Part 1, pp. 128–141, Nov. 2014.
- [113] M. Congedo, A. Barachant, and A. Andreev, “A New Generation of Brain-Computer Interface Based on Riemannian Geometry,” *arXiv:1310.8115 [cs, math]*, Oct. 2013.
- [114] E. Landhuis, “Neuroscience: Big brain, big data,” *Nature*, vol. 541, no. 7638, pp. 559–561, Jan. 2017.
- [115] R. T. Schirrmester, J. T. Springenberg, L. D. J. Fiederer, M. Glasstetter, K. Eggenberger, M. Tangermann, F. Hutter, W. Burgard, and T. Ball, “Deep learning with convolutional neural networks for EEG decoding and visualization,” *Hum. Brain Mapp.*, vol. 38, no. 11, pp. 5391–5420, Nov. 2017.
- [116] S. Biswal, J. Kulas, H. Sun, B. Goparaju, M. B. Westover, M. T. Bianchi, and J. Sun, “SLEEPNET: Automated Sleep Staging System via Deep Learning,” *arXiv:1707.08262 [cs]*, Jul. 2017.
- [117] R.-S. Huang, T.-P. Jung, and S. Makeig, “Tonic Changes in EEG Power Spectra during Simulated Driving,” in *Lecture Notes in Computer Science (LNCS)*, 2009, pp. 394–403.
- [118] S.-W. Chuang, L.-W. Ko, Y.-P. Lin, R.-S. Huang, T.-P. Jung, and C.-T. Lin, “Co-modulatory spectral changes in independent brain processes are correlated with task performance,” *Neuroimage*, vol. 62, no. 3, pp. 1469–1477, Sep. 2012.

- [119] R. Rosipal, B. Peters, G. Kecklund, T. Akerstedt, G. Gruber, M. Woertz, P. Anderer, and G. Dorffner, “EEG-Based Drivers’ Drowsiness Monitoring Using a Hierarchical Gaussian Mixture Model,” in *Foundations of Augmented Cognition*, D. D. Schmorrow and L. M. Reeves, Eds. Springer Berlin Heidelberg, 2007, pp. 294–303.
- [120] C. Zhao, C. Zheng, M. Zhao, Y. Tu, and J. Liu, “Multivariate autoregressive models and kernel learning algorithms for classifying driving mental fatigue based on electroencephalographic,” *Expert Systems with Applications*, vol. 38, no. 3, pp. 1859–1865, Mar. 2011.
- [121] C. S. Wei, Y. P. Lin, Y. T. Wang, T. P. Jung, N. Bigdely-Shamlo, and C. T. Lin, “Selective Transfer Learning for EEG-Based Drowsiness Detection,” in *2015 IEEE International Conference on Systems, Man, and Cybernetics (SMC)*, 2015, pp. 3229–3232.
- [122] E. J. Candès, X. Li, Y. Ma, and J. Wright, “Robust Principal Component Analysis?,” *J. ACM*, vol. 58, no. 3, p. 11:1–11:37, Jun. 2011.
- [123] P.-K. Jao, Y.-P. Lin, Y.-H. Yang, and T.-P. Jung, “Using robust principal component analysis to alleviate day-to-day variability in EEG based emotion classification,” in *2015 37th Annual International Conference of the IEEE Engineering in Medicine and Biology Society (EMBC)*, 2015, pp. 570–573.
- [124] Z. Lin, A. Ganesh, J. Wright, L. Wu, M. Chen, and Y. Ma, “Fast convex optimization algorithms for exact recovery of a corrupted low-rank matrix,” in *In Intl. Workshop on Comp. Adv. in Multi-Sensor Adapt. Processing, Aruba, Dutch Antilles*, 2009.